Frequency-Time Resource Allocation for Multiuser Uplink ISAC Systems

Zhitong Ni, *Member, IEEE*, J. Andrew Zhang, *Senior Member, IEEE*, Xiaojing Huang, *Senior Member, IEEE*, and Ren Ping Liu, *Senior Member, IEEE*

***Abstract*—Integrated sensing and communications (ISAC) is a promising technique for next-generation mobile networks, offering reduced device size, power consumption, cost, and improved spectrum efficiency. Full realization of such benefits relies on waveform design and resource allocation. This paper focuses on frequency-time (FT) resource allocation of multi-user uplink ISAC systems by minimizing the Cramér-Rao bound (CRB) of 5G new-radio signals. We first derive two types of CRBs for communications with respect to channel coefficients and parameters, respectively, and derive one CRB with respect to parameters for radar by removing the line-of-sight path and exploiting the shared parameters among different users' channels. Closed-form solutions to the FT resources are obtained under certain conditions for both radar and communication CRB minimizations, revealing the relationship and differences between the optimal radar and communication FT-resource allocations. Then, to balance the radar and communication CRB performance, we formulate two ISAC FT-resource optimization problems based on the two different communication CRBs and optimize FT resources accordingly. Finally, simulation results validate the effectiveness of the CRB optimization scheme.**

***Index Terms*—Integrated sensing and communication (ISAC), uplink sensing, Cramér-Rao bound (CRB), frequency-time resource**

I. Introduction

With the increasing influx of electronic devices in the market, the demand for network infrastructure continues to rise. These networks encompass various entities such as vehicles, home appliances, mobile devices, and other equipment that are equipped with sensors, software, and connectivity to facilitate data collection and exchange. There are several similarities between radar and communication systems regarding their hardware modules and signal processing methods [1]–[4]. In recent years, integrated sensing and communications (ISAC) have emerged as prevalent techniques, enabling seamless data exchange and facilitating information gathering in radio-silent environments.

ISAC systems have demonstrated immense potential across numerous applications. One notable application is in the context of sixth-generation (6G) cellular networks [5]–[7]. A concept known as perceptive mobile network (PMN) has been proposed, aiming to utilize communication links for environmental detection [8], [9]. The PMN concept was initially introduced in [6] and further elaborated upon in [7]. By enabling simultaneous uplink sensing and communication, the PMN allows user equipment (UE) to transmit signals while a base station (BS) receives them. Consequently, when a sufficient number of UEs are present, the radio-silent objects surrounding the BS can be comprehensively covered, enabling simultaneous data transmission and target detection. In a study by Huang et al. [10], an uplink channel estimation and sensing scheme based on deep learning was designed. Researchers in [11] conducted an analysis on the Cramér-Rao bound (CRB) for uplink ISAC and determined that the presence of multipath environments improves radar sensing accuracy. Additionally, parameter extractions, which involve selectively extracting the parameters of interest from the overall channel, can be utilized for radar channel acquisition [12]–[14].

The ISAC waveform holds the theoretical potential of doubling spectral efficiency (SE) by performing two functions simultaneously. However, in practical applications, a gap exists between the theoretically achievable SE and the actual SE due to the interference caused by the two individual waveforms. Numerous studies have focused on ISAC waveform optimization, considering various performance metrics such as mutual information (MI), signal-to-interference-plus-noise ratio (SINR), multi-user interference (MUI), and CRB. For instance, in [15], the authors investigated MI for a wideband ISAC system and maximized the weighted sum of the MI for both radar and communications. The authors in [16] developed a combined MI criterion that jointly designed waveform and power allocation to optimize performance in both radar and communications domains. Another approach presented in [17] allocated multiple users to interleaved subcarriers, effectively avoiding MUI, with SINR transformed into a convex metric. In [18], the authors proposed a method of separating the transmit antenna array into two sub-arrays and optimizing radar performance by imposing a SINR threshold constraint. In [19], the authors aimed to maximize radar SINR while maintaining a specific capacity for communication channels. Additionally, [20] introduced a sub-sampling matrix for radar as an objective function for optimization, further enhancing performance. These studies primarily focused on integrating spatial-domain waveforms. However, to increase the degree of freedom, further investigations into other multiplexing techniques are essential.

In the context of realizing ISAC functionality, frequency-time (FT) resource allocation also plays a crucial role, compared to space division multiplexing (SDM). In [21], the authors conducted experimental research on ISAC FT resource allocation with low transmit power, demonstrating promising sensing results and undisturbed communication capabilities.

Z. Ni, J. A. Zhang, X. Huang, and R. Liu are with the Global Big Data Technologies Centre, University of Technology Sydney, NSW, 2007, Australia (emails: zhitong.ni@uts.edu.au, andrew.zhang@uts.edu.au, xiaojing.huang@uts.edu.au, renping.liu@uts.edu.au).

Furthermore, the authors in [22] derived a Bayesian CRB and simplified it as an asymptotic CRB for a single-user ISAC system. It is worth noting that these works primarily focused on single-user systems, while the allocation of FT resources for multi-user systems remains an unexplored area. This observation serves as motivation for our investigation into FT-domain resource allocation for multi-user systems.

Similar to many joint waveform optimization works for communications-centric ISAC [21], [22], we aim to optimize resource allocation in orthogonal frequency division multiplexing (OFDM) systems, which are widely used in modern communication networks. The optimization can lead to a desired tradeoff between communication and sensing performance, without requiring significant changes in existing communications infrastructure. Such optimization can typically be achieved by minimizing minimum-mean-squared error (MMSE) and Cramér-Rao bound (CRB) [22], [23]. MMSE serves as a widely used metric to evaluate the performance of estimation algorithms in radar and communication systems. By employing MMSE as the optimization goal for waveform design, the system's ability to resolve detection angles, ranges, and velocities can be enhanced [24]. However, MMSE is typically result-oriented and varies according to different estimation schemes, posing challenges when attempting to bridge the gap between ideal and practical waveforms. The CRB, on the other hand, represents a fundamental limit that defines the minimum achievable variance of MMSE. Optimizing the CRB is crucial for evaluating estimation algorithms' performance and providing insights into estimator design. In the study of [25], null-space projection methods were investigated for radar, and the CRB was utilized to evaluate target direction performance. The authors in [26] focused on the millimeter-wave ISAC system and optimized the waveform for partially-connected hybrid arrays. It is important to note that the CRB is only applicable to unbiased estimators. In cases where parameters are mixed with offsets and become biased, deriving a CRB becomes invalid. Additionally, due to the complexity of the CRB matrix expression, the optimization problem often becomes intractable and is typically transformed into a semi-definite programming (SDP) problem, where the inverse of the CRB matrix, known as the Fisher information matrix (FIM), becomes the independent variable. To simplify the optimization problem, various strategies can be employed, such as maximizing the smallest eigenvalue of the FIM [27].

The uplink PMN channel offers a unique opportunity to integrate radar and communication signals through shared channel parameters. While existing research predominantly focuses on integrating signals using SDM techniques, there is a lack of comprehensive exploration of FT resource optimization in the FT domain, especially for multi-user systems. To leverage the high estimation accuracy of FT-domain signals, the CRB emerges as a natural choice for FT resource optimization. This paper aims to investigate the FT resource allocation by minimizing the CRB. The research specifically addresses the scenario of multi-user uplink PMN, wherein multiple UEs communicate with a single BS across different FT resources. Our approach involves deriving several different CRBs for communications and radar and subsequently optimizing FT-domain bins accordingly. The contributions of this paper are listed below:

- We derive two uplink CRBs of communications with respect to (w.r.t.) either channel coefficients or parameters, and optimize the FT resources for multiple UEs. The closed-form solution is obtained within a large number of paths.
- We derive the uplink CRB of radar by jointly processing all UEs' signals together, and optimize the FT resources for multiple UEs. We also obtain a closed-form solution when the number of FT resources is sufficiently large.
- We formulate two types of ISAC FT resource optimization problems depending on whether the channel coefficients are correlated or not.

TABLE I
SUMMARIZATION FOR MAIN SYMBOLS USED IN THIS PAPER.

Parameter	Meaning
$U(u)$	number (index) of UEs
$N(n)$	number (index) of antennas at BS
$Q(q)$	number (index) of independent parameters
$L(l)$	number (index) of NLOS paths
$M(m)$	number (index) of time slots
$G(g)$	number (index) of subcarriers
T	length of an OFDM symbol, e.g., 0.25μs
T_{C}	length of CP, e.g., 0.125μs
T'	interval of two time packets, e.g., 1 ms
Λ_u/S_u	FT bins / size of FT bins
f_c	carrier frequency, e.g., 2.4 GHz
P_o	Power constraints, e.g., 3 W
V	$T'f_c$
X	Baseband symbols: $X[g,m]$
α	path gain: $\alpha_{l,u}, \alpha_l$, and α_q
ν	Doppler shift: $\nu_{l,u}, \nu_l$, and ν_q
τ	delay: $\tau_{l,u}, \tau_l$, and τ_q
ω	equivalent AoA: $\omega_{l,u}, \omega_l$, and ω_q
c	communication: $X^c, \mathbf{F}_c^u$, and $\mathbf{F}_c^A$
r	radar: X^r and $\mathbf{F}_\psi^r$
y	received signal: $y_n[g,m]$
z	noise: $z_n[g,m], z_n^u$, and z^u
$\boldsymbol{\xi}$	channel coefficients for communications
$\boldsymbol{\psi}$	Delay-Doppler exponents, defined in (7)
$\boldsymbol{\theta}$	all parameters
$\boldsymbol{\phi}$	all parameters except path gains

Notations: $\mathbf{a}$ denotes a vector, $\mathbf{A}$ denotes a matrix, italic English letters like N and lower-case Greek letters like α are scalar. $\mathbf{A}^T, \mathbf{A}^H, \mathbf{A}^*$, $\mathbf{A}^{-1}$, and $\mathbf{A}^\dagger$ represent transpose, conjugate transpose, conjugate, inverse and pseudo inverse, respectively. $\|\mathbf{A}\|_F$ is Frobenius norm of a matrix. $\mathrm{diag}(\mathbf{A})$ is a vector of which entries are the diagonal entries of $\mathbf{A}$ and $\mathrm{diag}(\mathbf{a})$ is a diagonal matrix of which diagonal entries are $\mathbf{a}$. $\frac{\partial \mathbf{a}}{\partial \mathbf{b}} \triangleq \left[\frac{\partial \mathbf{a}}{\partial b_1}, \cdots, \frac{\partial \mathbf{a}}{\partial b_L}\right]$ with $\mathbf{b} = [b_1, \cdots, b_L]^T$. $\otimes$, $\odot$, and $\circ$ denote the Kronecker product, Khatri-Rao product, and Hadamard product, respectively. The adopted symbols are summarized in Table 1.

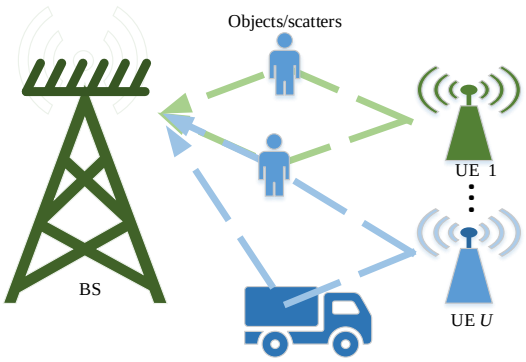

Fig. 1. Illustration of uplink sensing in PMN, where multiple UEs communicate with one BS and the BS realizes ISAC functions. Each UE's transmitted signal can impinge on either the same or different objects. The received signals contain partial information about radio-silent objects.

Section II presents the adopted multi-user uplink OFDM system and channel models in ISAC scenarios. Section III derives the CRBs and presents the corresponding optimization problems for communications, radar, and ISAC functions. Section IV provides the simulation results and Section V concludes this paper.

II. System and Channel Models

A. System Model

We consider an uplink multi-user ISAC system, as shown in Fig. 1, where dashed curves of different colors represent scattered signals from different UEs. There are U UEs communicating with one BS. Each UE has one antenna. The BS has a uniform linear array (ULA) of N antennas. The transmitted signals are shared by communications and sensing, referring to the 5G new-radio (NR) signal structure. This standardized signal structure provides a robust and versatile framework that aligns with the capabilities and requirements of our system. In the 5G NR signal structure, the pilot symbol is known as a demodulation reference signal (DMRS) block. In this paper, we use DMRS type of pilot symbols for channel estimation in communications and sensing.

Each baseband OFDM symbol has G subcarriers with a subcarrier interval of $1/T$, and T is the length of an OFDM symbol. Each OFDM symbol is prepended by a cyclic prefix (CP) of period $T_{\rm C}$. We assume that M OFDM pilot symbols are transmitted in a coherent processing interval (CPI), and the interval between the mth and $(m+1)$th pilot symbols is T'. For simplicity, we assume that T' is an integral time of $T+T_{\rm C}$.

Multiple UEs are served within G subcarriers and M time slots. For the uth UE, the BS allocates a segment of the FT resources,

$$\Lambda_u = \{g_u, m_u | 0 \le g_u \le G-1, 0 \le m_u \le M-1\}, \quad (1)$$

where g_u and m_u denote the indices of subcarriers and time slots, respectively, which are allocated for the uth UE. To avoid multi-user interference, the FT resources are non-overlapped among multiple UEs, that is, $\Lambda_u \bigcap \Lambda_{u'} = \emptyset, \forall 1 \le u, u' \le U$. Hence, the adopted system is an orthogonal frequency division multiple access (OFDMA) system. Note that the orthogonality between allocated FT resources for different UEs is guaranteed by the use of CP and the stringent timeslot structure in mobile networks, without requiring additional guarding intervals.

The transmitted ISAC signal is given by

$$x_u(t) = \sum_{g=0}^{G-1}\sum_{m=0}^{M-1} e^{j2\pi(g/T+f_c)t} \text{rect}\left(\frac{t-mT'}{T+T_{\rm C}}\right) \epsilon_u^{g,m} X[g,m], \quad (2)$$

where f_c is the carrier frequency, $\text{rect}\left(\frac{t}{T+T_{\rm C}}\right)$ denotes a rectangular window of length $(T+T_{\rm C})$, $\epsilon_u^{g,m}$ is either 1 or 0 with 1 indicating that the (g,m)-th FT bin belongs to UE u, and $X[g,m]$ is a complex value denoting the baseband pilot symbol. When the transmitted signal is optimized for radar (communication) solely, we rewrite $X[g,m]$ as $X^r[g,m]$ ($X^c[g,m]$). We let $\sum_{g=0}^{G-1}\sum_{m=0}^{M-1} \epsilon_u^{g,m}|X[g,m]|^2 \le P_o$ with P_o the transmit power constraint for each UE. In this paper, GPS-disciplined oscillators are adopted among the UEs, such that the transmitted signals are synchronized without timing offsets and carrier-frequency offsets.

Note that the OFDM symbols in a CPI are collected in the (G,M) FT bins at BS. To improve the sensing accuracy, the FT bins among multiple UEs can be jointly processed when the parameters of different UEs are related. The relationship will be illustrated as follows.

B. Channel Model

As shown in Fig. 1, the BS detects all the objects for radar sensing and estimates the communication channel for each UE. In the uplink ISAC scenario, the radar channel and communication channel are the same but radar is generally not interested in estimating the line-of-sight (LOS) path between UE and BS, if it is present. Additionally, channel coefficients are the main concern for communication channel estimation, while radar mainly focuses on estimating the sensing parameters in the channel, such as delay, Doppler, and angle of arrival (AoA). The adopted ISAC channel model is a limited-scattered single-input multi-output (SIMO) geometry channel, given by

$$\mathbf{H}_u(t) = \sum_{l=0}^{L} \alpha_{l,u}\delta\left(t-\tau_{l,u}+\nu_{l,u}t\right)\mathbf{a}(\omega_{l,u}), \quad (3)$$

where $\alpha_{l,u}$, $\tau_{l,u}$, and $\nu_{l,u}$ are the complex path gain, propagation delay, and Doppler shift in the lth path between the uth UE and BS, respectively, $\delta(t)$ is an impulse signal, and $\mathbf{a}(\omega_{l,u}) = \exp[j\omega_{l,u}(0,1,\cdots,N-1)]^T$ is the array response vector of size $N\times 1$ with $\omega_{l,u} = \pi\sin(\theta_{l,u})$ and $\theta_{l,u}$ the AoA. We let the path of $l=0$ be the LOS path that contains no information about radio-silent objects. When $l \ge 1$, we let the lth path be the non-line-of-sight (NLOS) path reflected from the lth object.

It is noted that the number of objects is limited and generally less than the total number of paths LU. In this paper, we aim to disclose the relationship of channels among multiple UEs. Hence, we assume that some of the NLOS paths of

different UEs share the same parameters. When different UEs' transmitted signals impinge on the same object, the corresponding AoAs and Doppler shifts are the same, that is,

$$\omega_{l,u} = \omega_{l',u'}, \nu_{l,u} = \nu_{l',u'}, \exists u' \neq u, \tag{4}$$

where l' denotes the index of the NLOS path. As for delays, we note that different UEs would have different delays for all NLOS paths because the delays from each UE to the object are also included in $\tau_{l,u}$. This makes $\tau_{l,u}$ become an independent variable even if the impinged object is the same one. In spite of the particularity of delays, we can still integrate multiple UEs' signals together to obtain the shared parameters. Here, for notational simplicity, we define Q as the number of independent parameters (AoAs/Dopplers/delays). In the single-user systems, we note that Q equals the number of objects. When the objects are close to the UE and distant from the BS, Q is approximately equal to the number of objects too.

The received signal is transformed into the frequency domain via G-point fast-Fourier-transform after the CP is removed. The received FT-domain signal of the nth antenna at the (g,m)-th FT bin is

$$\begin{aligned} & y_n[g,m] \\ =& \sum_{u=1}^{U}\sum_{l=1}^{L} \alpha_{l,u} e^{jn\omega_{l,u}} e^{j2\pi m V \nu_{l,u}} e^{-j2\pi g \tau_{l,u}/T} \epsilon_u^{g,m} X[g,m] \\ & + z_n[g,m], \end{aligned} \tag{5}$$

where $V = T' f_c$ is a coefficient that has a unit of 1, and $z_n[g,m]$ is a complex additive-white-Gaussian-noise (AWGN) with zero mean and variance of σ^2. In this paper, we only consider FT resource optimizations based on CRB minimizations. Hence, the power distribution, $|X[g,m]\epsilon_u^{g,m}|$, is the FT resources/bins to be optimized.

III. FT-Bin Optimizations Based on CRB Minimizations

In this section, we present the derivation of various CRBs tailored for uplink multi-user systems. Our objective is to optimize the baseband FT bins by minimizing the CRBs. The FT bins of all UEs span the entire range of $g \in \{0, \cdots, G-1\}$ and $m \in \{0, \cdots, M-1\}$. It is noteworthy that each UE exclusively transmits signals from its designated FT bins. Our optimization efforts focus on two distinct aspects: communication and radar. For communication, each UE seeks an accurate communication channel solely within its assigned FT bins. On the other hand, radar necessitates precise parameters of objects across the entire channel. In Subsection III-A, we derive the CRB specific to each UE for communication and subsequently optimize the FT bin exclusively for communication purposes. The resulting CRBs exhibit two distinct forms contingent on whether the independent variables are channel coefficients or sensing parameters within the communication channels. In Subsection III-B, we extend our analysis to derive a CRB tailored for radar sensing. Here, we exploit the relationship among parameters and optimize the FT bin exclusively for radar sensing. In Subsection III-C, we introduce two ISAC FT-bin optimization problems and then derive the corresponding optimal solutions to enhance the overall performance of the system.

A. CRB of Communications

We derive the CRB for each UE's individual channel estimation, assuming that the signals of all UEs are allocated separately at different FT bins. In the context of communication channel estimation, the CRB for each UE's individual channel can be determined with respect to either channel coefficients or parameters such as path gains, delays, AoAs, and Doppler shifts.

Here, we let $X[g,m] = X^c[g,m]$ to highlight that the signal is optimized by considering the communication performance only. To derive the CRB of the uth UE, we can stack the measurements of $y_n[g,m]$ as

$$\begin{aligned} \mathbf{y}_n^u &= [y_n[0,0], \cdots, y_n[G-1,0], \cdots, y_n[G-1,M-1]]^T \circ \boldsymbol{\epsilon}^u \\ &= \sum_{l=0}^{L} \alpha_{l,u} e^{jn\omega_{l,u}} \boldsymbol{\psi}(\nu_{l,u}, \tau_{l,u}) \circ \mathbf{c} \circ \boldsymbol{\epsilon}^u + \mathbf{z}_n \circ \boldsymbol{\epsilon}^u \\ &\triangleq \sum_{l=0}^{L} \alpha_{l,u} e^{jn\omega_{l,u}} \boldsymbol{\psi}(\nu_{l,u}, \tau_{l,u}) \circ \boldsymbol{\epsilon}^u \circ \mathbf{c} + \mathbf{z}_n^u, \end{aligned} \tag{6}$$

where $\mathbf{c} = [X^c[0,0], \cdots, X^c[G-1,0], \cdots, X^c[G-1,M-1]]^T$ is the communication FT-bin vector to be optimized, the entries of $\boldsymbol{\epsilon}^u$ are $\epsilon_u^{g,m}$ with 1 indicating that the (g,m)-th FT bin belongs to Λ_u and 0 indicating not, $\mathbf{z}_n^u = \mathbf{z}_n \circ \boldsymbol{\epsilon}^u$ is a noise vector, and

$$\begin{aligned} \boldsymbol{\psi}(\nu,\tau) =& \exp\left[j2\pi(V\nu 0 - 1/T\tau 0, \cdots, V\nu 0 - 1/T\tau(G-1),\right. \\ & \left. \cdots, V\nu(M-1) - 1/T\tau(G-1))\right]^T \\ =& \exp\left[j2\pi(V\nu(0,\cdots,M-1))\right]^T \\ & \otimes \exp\left[j2\pi(\tau/T(0,\cdots,G-1))\right]^T, \end{aligned} \tag{7}$$

with ν and τ auxiliary values.

To include the AoA impacts, we stack $\mathbf{y}_n^u$ into a vector $\mathbf{y}^u$ and rewrite $\mathbf{y}^u$ into a concise form, given by

$$\begin{aligned} & \mathbf{y}^u \\ =& \left[(\mathbf{y}_1^u)^T, \cdots, (\mathbf{y}_N^u)^T\right]^T \\ =& \sum_{l=0}^{L} \alpha_{l,u} \mathbf{a}(\omega_{l,u}) \otimes \boldsymbol{\psi}(\nu_{l,u}, \tau_{l,u}) \circ (\mathbf{1}_N \otimes \boldsymbol{\epsilon}^u) \circ (\mathbf{1}_N \otimes \mathbf{c}) + \mathbf{z}^u \\ =& \mathrm{diag}(\mathbf{1}_N \otimes \mathbf{c})\mathbf{h}^u + \mathbf{z}^u, \end{aligned} \tag{8}$$

where $\mathbf{a}(\omega_{l,u})$ is an $N \times 1$ array response vector, $\mathbf{z}^u$ is the assembly of $\mathbf{z}_n^u$ w.r.t. n, and $\mathbf{h}^u = \sum_{n=1}^{N}\sum_{l=0}^{L} \alpha_{l,u} \mathbf{a}(\omega_{l,u}) \otimes \boldsymbol{\psi}(\nu_{l,u}, \tau_{l,u}) \circ (\mathbf{1}_N \otimes \boldsymbol{\epsilon}^u)$. Note that the received signal vector is the sum of channel $\mathbf{h}^u$ and noise $\mathbf{z}^u$.

For communications, the precision of the non-zero entries in $\mathbf{h}^u$ holds paramount importance. When dealing with a limited number of paths, the entries of $\mathbf{h}^u$ lack independence and identical distribution (i.i.d). In such instances, it becomes feasible to derive the CRB with respect to the parameters. The resulting CRB closely aligns with that of radar, and the optimization methods follow a similar pattern. On the contrary, when confronted with a substantial number of paths,

the entries of $\mathbf{h}^u$ can be reasonably assumed to be i.i.d. In such scenarios, it is possible to derive the CRB w.r.t. either parameters or channel coefficients.

1) CRB of communications w.r.t. channel coefficients: We derive the CRB with the assumption that the entries of $\mathbf{h}^u$ are i.i.d, which is valid when L is large enough. The normalized entries of $\mathbf{h}^u$ are formed into a real-valued vector, denoted as $\boldsymbol{\xi}^u = \|\mathbf{h}^u\|_F^{-1}[\mathrm{Re}(\mathbf{h}^u)^T, \mathrm{Im}(\mathbf{h}^u)^T]^T$. Since the channel coefficients are i.i.d., each entry of $\mathbf{h}^u$ to be estimated has one measurement only, i.e., $y_n[g,m]$.

Referring to (33) of [23], the FIM is a sum of two individual parts with one part specific to the derivatives of noise. In general, the noise is uncorrelated among the FT bins, and the FIM can be simplified by removing the derivatives of noise. The adopted FIM is a so-called asymmetric FIM. The corresponding FIM is given by

$$\mathbf{F}_c^u = \sum_{i=1}^{S_u} 2\mathrm{Re}\{D_{\xi_i^u}(h_i^u)^H \sigma^{-2} D_{\xi_i^u}(h_i^u)\}, \tag{9}$$

where S_u is the number of non-zero entries of $\mathbf{h}^u$, i.e., $S_u = N|\Lambda_u|$, g_i^u and ξ_i^u are the ith non-zero entry of $\mathbf{h}^u$ and $\boldsymbol{\xi}^u$, respectively, and

$$D_{\xi_i^u}(h_i^u) = \frac{\partial h_i^u}{\partial \xi_i^u}. \tag{10}$$

Note that since each entry only has one measurement, $\mathbf{F}_c^u$ is a scalar that is calculated as

$$\begin{aligned}\mathbf{F}_c^u &= 2\sigma^{-2} \sum_{i=1}^{S_u} \mathrm{Re}\left\{ \left(\frac{\partial h_i^u}{\partial \xi_i^u}\right)^H \frac{\partial h_i^u}{\partial \xi_i^u} \right\} \\ &= 2\sigma^{-2} \|\mathbf{h}^u\|_F^2 (\mathbf{1}_N \otimes \mathbf{c} \circ \boldsymbol{\epsilon}^u)^H \mathbf{1}_N \otimes \mathbf{c} \circ \boldsymbol{\epsilon}^u. \end{aligned} \tag{11}$$

The FT-bin optimization problem is formulated as

$$\begin{aligned} &\mathbf{c}^\star, \boldsymbol{\epsilon}^{u\star} = \arg \min_{\mathbf{c}} \max_{\boldsymbol{\epsilon}^u} (-t_u) \\ &\text{s.t.} \quad \mathbf{F}_c^u \geq t_u, \|\mathbf{c} \circ \boldsymbol{\epsilon}^u\|_F^2 \leq P_o, \end{aligned} \tag{12}$$

where t_u is an auxiliary value. The optimal solution is $\mathbf{c} \circ \boldsymbol{\epsilon}^u = \boldsymbol{\epsilon}^u / \lambda^u$, where λ^u is proportional to $\|\boldsymbol{\epsilon}^u\|_F^2$.

It should be highlighted that the number of paths to be estimated is related to the value of M and G. In general, M determines the maximal number of Doppler shifts to be estimated and G determines the maximal number of delays to be estimated. Therefore, as long as L does not exceed either M or G, we can derive the CRB w.r.t. the parameters, shown below.

2) CRB of communications w.r.t. sensing parameters: For communications, we derive the CRB w.r.t. all parameters including the path gains. For simplicity of exposition, we drop the subscript u here. All parameters are stacked into a real-valued vector, denoted as $\boldsymbol{\theta} = [\mathrm{Re}(\boldsymbol{\alpha})^T, \mathrm{Im}(\boldsymbol{\alpha})^T, \boldsymbol{\nu}^T, \boldsymbol{\tau}^T, \boldsymbol{\omega}^T]^T$, with $\boldsymbol{\alpha} = [\alpha_0, \cdots, \alpha_L]^T$, $\boldsymbol{\nu} = [\nu_0, \cdots, \nu_L]^T$, $\boldsymbol{\tau} = [\tau_0, \cdots, \tau_L]^T$, and $\boldsymbol{\omega} = [\omega_0, \cdots, \omega_L]^T$.

The FIM of all parameters is given by

$$\mathbf{F}_c^A = 2\mathrm{Re}\{D_{\boldsymbol{\theta}}(\mathbf{g})^H \sigma^{-2} D_{\boldsymbol{\theta}}(\mathbf{g})\}, \tag{13}$$

where

$$\begin{aligned} &D_{\boldsymbol{\theta}}(\mathbf{g}) \\ &= \left[D_{\mathrm{Re}(\boldsymbol{\alpha})}(\mathbf{g})^T, D_{\mathrm{Im}(\boldsymbol{\alpha})}(\mathbf{g})^T, D_{\boldsymbol{\nu}}(\mathbf{g})^T, D_{\boldsymbol{\tau}}(\mathbf{g})^T, D_{\boldsymbol{\omega}}(\mathbf{g})\right]^T, \end{aligned} \tag{14}$$

and $\mathbf{g} = \sum_{u=1}^{U} \mathbf{h}^u$ is the integrated channel vector. The FT bins only have the main impacts on delay and Doppler shift. Hence, we assemble the subblocks w.r.t. delay and Doppler shift together. The corresponding delay-Doppler FIM has 2×2 subblocks, given by

$$\mathbf{F}_{\boldsymbol{\psi}} = \begin{bmatrix} \mathbf{F}_{\boldsymbol{\nu},\boldsymbol{\nu}} & \mathbf{F}_{\boldsymbol{\nu},\boldsymbol{\tau}} \\ \mathbf{F}_{\boldsymbol{\tau},\boldsymbol{\nu}} & \mathbf{F}_{\boldsymbol{\tau},\boldsymbol{\tau}} \end{bmatrix}. \tag{15}$$

Then, (13) can be separated into 3×3 subblocks, given by

$$\mathbf{F}_c^A = \begin{bmatrix} \mathbf{F}_{\boldsymbol{\alpha},\boldsymbol{\alpha}} & \mathbf{F}_{\boldsymbol{\alpha},\boldsymbol{\omega}} & \mathbf{F}_{\boldsymbol{\alpha},\boldsymbol{\psi}} \\ \mathbf{F}_{\boldsymbol{\omega},\boldsymbol{\alpha}} & \mathbf{F}_{\boldsymbol{\omega},\boldsymbol{\omega}} & \mathbf{F}_{\boldsymbol{\omega},\boldsymbol{\psi}} \\ \mathbf{F}_{\boldsymbol{\psi},\boldsymbol{\alpha}} & \mathbf{F}_{\boldsymbol{\psi},\boldsymbol{\omega}} & \mathbf{F}_{\boldsymbol{\psi}} \end{bmatrix}, \tag{16}$$

where the subblocks are expressed in Appendix A and Appendix B. The FIM subblocks w.r.t. angle, delay, and Doppler shift are presented in Appendix A, and the FIM subblocks w.r.t. path gains are presented in Appendix B. We separate the path gains from other parameters as the radar sensing only requires angle, delay, and Doppler shift whereas the communication requires all parameters.

We can optimize the FT bins based on the CRB minimizations of delay-Dopplers, and formulate the FT-bin optimization problem as

$$\begin{aligned} &\mathbf{c}^\star = \arg \min_{\mathbf{c}} (-t) \\ &\text{s.t.} \quad \mathbf{F}_{\boldsymbol{\psi}} \succeq t\mathbf{I}, \mathbf{F}_{\boldsymbol{\alpha},\boldsymbol{\alpha}} \succeq t_\alpha \mathbf{I}, \mathbf{F}_{\boldsymbol{\omega},\boldsymbol{\omega}} \succeq t_\omega \mathbf{I}, \|\mathbf{c}\|_F^2 \leq P_o, \end{aligned} \tag{17}$$

where $\mathbf{c} = [X^c[0,0], \cdots, X^c[G-1,0], \cdots, X^c[G-1,M-1]^T$ is the FT bins for communication, t is an auxiliary value, and t_α and t_ω are the thresholds used to constrain the FIM of path gains and AoAs, respectively. The problem above can be solved by using SDP w.r.t. $\mathbf{X} = \mathrm{diag}(\mathbf{c})^H \mathrm{diag}(\mathbf{c})$.

B. CRB of Radar Sensing

From the former subsection, it should be highlighted that when using different independent variables, the corresponding CRBs are different. For radar sensing, the adopted grids of measurements occupy the whole range of m and g. Here, we consider the CRB of delays, Dopplers, and AoAs, while path gains are omitted for radar sensing.

Since the radar focuses on estimating the parameters w.r.t. a limited number of objects, it is not necessary to derive the CRB for multiple UEs individually. Without loss of generality, we derive the CRB of single-user systems first. Then, the CRB of multiple UEs can be easily obtained by transforming the expression of single-user CRB.

1) Radar CRB of single-user system: We model the channel measurements as a sum of the channel of interest, LOS path, and AWGN. Here, we let $X[g,m] = X^r[g,m]$ to highlight that the signal is optimized for radar sensing only. To derive the

CRB, we stack the measurements of $y_n[g,m]$ from $[g,m]=[0,0]$ to $[g,m]=[G-1,M-1]$ into an $MG\times 1$ vector,

$$\begin{aligned}\mathbf{y}_n &= [y_n[0,0],\cdots,y_n[G-1,0],\cdots,y_n[G-1,M-1]]^T\\ &=\sum_{l=1}^{L}\alpha_l e^{jn\omega_l}\boldsymbol{\psi}(\nu_l,\tau_l)\circ\mathbf{r}+\alpha_0 e^{jn\omega_0}\boldsymbol{\psi}(\nu_0,\tau_0)\circ\mathbf{r}+\mathbf{z}_n\\ &=\sum_{q=1}^{Q}\alpha_q e^{jn\omega_q}\boldsymbol{\psi}(\nu_q,\tau_q)\circ\mathbf{r}+\alpha_0 e^{jn\omega_0}\boldsymbol{\psi}(\nu_0,\tau_0)\circ\mathbf{r}+\mathbf{z}_n,\end{aligned} \tag{18}$$

where $\mathbf{r}=[X^r[0,0],\cdots,X^r[G-1,0],\cdots,X^r[G-1,M-1]^T]$ is the radar FT-bin vector to be determined. Note that in a single-user system, both Q and L equal the number of objects.

Similar to the former subsection, we stack $\mathbf{y}_n$ into a vector $\mathbf{y}=\left[\mathbf{y}_1^T,\cdots,\mathbf{y}_N^T\right]$ and rewrite $\mathbf{y}$ into a concise form as

$$\begin{aligned}\mathbf{y}&=\left(\sum_{l=1}^{L}\alpha_l\mathbf{a}(\omega_l)\otimes\boldsymbol{\psi}(\nu_l,\tau_l)+\mathbf{i}\right)\circ(\mathbf{1}\otimes\mathbf{r})+\mathbf{z}\\ &\triangleq\mathbf{g}+\mathrm{diag}(\mathbf{1}\otimes\mathbf{r})\mathbf{i}+\mathbf{z},\end{aligned} \tag{19}$$

where $\mathbf{i}=\alpha_0\mathbf{a}(\omega_0)\otimes\boldsymbol{\psi}(\nu_0,\tau_0)$ denotes the intereference generated by the LOS path, and $\mathbf{z}$ is the noise vector. Note that the received signal vector contains channel $\mathbf{g}$, interference $\mathbf{i}$, and noise $\mathbf{z}$.

It should be highlighted that $\mathbf{i}$ is caused by the LOS path that can be obtained using specific estimators. For example, the authors in [28] used an add-minus suppression method to remove the LOS path from the received signal. In this case, $\mathbf{i}$ can be perfectly or partially removed from the received signal vector. Then, the received signal is given by

$$\mathbf{y}'=\mathbf{g}+\mathrm{diag}(\mathbf{1}\otimes\mathbf{r})\mathbf{d}+\mathbf{z}, \tag{20}$$

with $\mathbf{d}=\mathbf{i}-\hat{\mathbf{i}}$. The CRB without the parameters of the LOS path is lower than the CRB with including the LOS path, which is because the LOS path introduces one more group of parameters that are not necessary to be obtained for radar.

All parameters used for radar sensing are formed into a real-valued vector, denoted as $\boldsymbol{\theta}=[\boldsymbol{\psi}^T,\boldsymbol{\omega}^T]^T$, with $\boldsymbol{\psi}=[\boldsymbol{\nu},\boldsymbol{\tau}]$, $\boldsymbol{\nu}=[\nu_1,\cdots,\nu_L]^T$, $\boldsymbol{\tau}=[\tau_1,\cdots,\tau_L]^T$, and $\boldsymbol{\omega}=[\omega_1,\cdots,\omega_L]^T$. Compared with the communication vector, the index of l starts from 1 instead of 0. The FIM of radar sensing is given by

$$\mathbf{F}=2\mathrm{Re}\{D_{\boldsymbol{\phi}}(\mathbf{g})^H\mathbf{C}^{-1}D_{\boldsymbol{\phi}}(\mathbf{g})\}, \tag{21}$$

with

$$D_{\boldsymbol{\phi}}(\mathbf{g})=\frac{\partial\mathbf{g}}{\partial\boldsymbol{\phi}}=\left[D_{\boldsymbol{\nu}}(\mathbf{g})^T,D_{\boldsymbol{\tau}}(\mathbf{g})^T,D_{\boldsymbol{\omega}}(\mathbf{g})\right]^T, \tag{22}$$

and

$$\begin{aligned}\mathbf{C}&=\mathbb{E}\big((\mathrm{diag}(\mathbf{1}\otimes\mathbf{r})\mathbf{d}+\mathbf{z})(\mathrm{diag}(\mathbf{1}\otimes\mathbf{r})\mathbf{d}+\mathbf{z})^H\big)\\ &=\mathbf{I}\otimes\mathbf{X}\mathbf{d}\mathbf{d}^H+\sigma^2\mathbf{I},\end{aligned} \tag{23}$$

where $\mathbf{X}=\mathrm{diag}(\mathbf{r})^H\mathrm{diag}(\mathbf{r})$. The subblocks of $\mathbf{F}$ are omitted since they can be referred to Appendix A. The differences are: 1) the correlation matrix is $\mathbf{C}$ instead of $\sigma^2\mathbf{I}$; 2) the derivatives only include the parameters of objects, i.e., $1\le l\le L$.

Similar to Section III-A2, the optimization problem is formulated as

$$\begin{aligned}&\mathbf{r}=\arg\min_{\mathbf{r}}\quad -t\\ &\text{s.t.}\quad \mathbf{F}^r_{\boldsymbol{\psi}}\succeq t\mathbf{I},\mathbf{F}^r_{\boldsymbol{\omega},\boldsymbol{\omega}}\succeq t_\omega\mathbf{I},\|\mathbf{r}\|_F^2\le P_o,\end{aligned} \tag{24}$$

where $\mathbf{F}^r_{\psi}$ is given by

$$\mathbf{F}^r_{\psi}=\begin{bmatrix}\mathbf{F}_{\boldsymbol{\nu},\boldsymbol{\nu}} & \mathbf{F}_{\boldsymbol{\nu},\boldsymbol{\tau}}\\ (\mathbf{F}_{\boldsymbol{\nu},\boldsymbol{\tau}})^H & \mathbf{F}_{\boldsymbol{\tau},\boldsymbol{\tau}}\end{bmatrix}. \tag{25}$$

Due to the existence of interference, it is quite challenging to solve the problem above. Fortunately, as will be shown in Corollary 1, the optimal radar FT bin without interference shows a sparse property, that is, there are a limited number of non-zero elements in the optimal solutions. Hence, the optimal radar FT-bin allocations without the interference of the LOS path can be solved using convex optimization methods.

Now, we omit the interference and propose the following Proposition 1.

Proposition 1. *The optimal non-limited FT-bin matrix, $\mathbf{X}^\star$, is a three-layer diagonal matrix when the number of antennas is 1 and the number of FT bins, MG, is sufficiently larger than Q^2.*

The proof is provided in Appendix C.

Corollary 1. *The optimal FT-bin matrix, $\mathbf{X}^\star$, only has $(DQ)^2$ non-zero entries with $(DQ)^2$ the size of FIM.*

Proof. According to Proposition 1, to form an arbitrary FIM of dimension $DQ\times DQ$, denoted as $\mathbf{F}$, we can construct the matrices, $\mathbf{U}_{\mathrm{d}}$ and $\mathbf{U}_{\mathrm{nd}}$, as in Appendix C. Then, the entries of the matrix can be obtained by solving

$$[\mathbf{U}_{\mathrm{d}},\mathbf{U}_{\mathrm{nd}}][x_1,\cdots,x_{MG-2},y_1,\cdots,y_{MG-2}]^T=\mathrm{vec}(\mathbf{F}), \tag{26}$$

Since $[\mathbf{U}_{\mathrm{d}},\mathbf{U}_{\mathrm{nd}}]$ has a rank of $(DQ)^2$, there are only $(DQ)^2$ non-zero entries, which ends the proof. □

According to the definition of $\mathbf{X}$ in Appendix A, i.e., $\mathbf{X}=\mathrm{diag}(\mathbf{x})^2$, we note that the FT-bin matrix is a diagonal matrix and thus needs to be truncated with retaining the diagonal entries only. Therefore, we propose Theorem 1 to obtain the closed-form solution to the optimization problem of (24).

Theorem 1. *When the numbers of subcarriers and time slots, M and G, are sufficiently large and $N=1$, the closed-form solution of the optimal radar FT bin exists.*

Proof. Observing the definition of $\mathbf{X}$, $\mathbf{X}=\mathrm{diag}(\mathbf{x})^H\mathrm{diag}(\mathbf{x})$, which is a diagonal matrix with the dth diagonal entry being x_d. Referring to (52), (53), and (54), the FIM is rewritten as

$$\begin{aligned}\mathbf{F}^r_{\psi}&=\begin{bmatrix}\mathbf{F}_{\boldsymbol{\nu},\boldsymbol{\nu}} & \mathbf{F}_{\boldsymbol{\nu},\boldsymbol{\tau}}\\ \mathbf{F}_{\boldsymbol{\tau},\boldsymbol{\nu}} & \mathbf{F}_{\boldsymbol{\tau},\boldsymbol{\tau}}\end{bmatrix}\\ &=2\sigma^{-2}\mathrm{Re}\left\{\sum_{d=1}^{MG}x_d\begin{bmatrix}\mathbf{M}^d_{\boldsymbol{\nu},\boldsymbol{\nu}} & \mathbf{M}^d_{\boldsymbol{\nu},\boldsymbol{\tau}}\\ \mathbf{M}^d_{\boldsymbol{\tau},\boldsymbol{\nu}} & \mathbf{M}^d_{\boldsymbol{\tau},\boldsymbol{\tau}}\end{bmatrix}\right\},\end{aligned} \tag{27}$$

where x_d, $d\in\{1,\cdots,MG\}$, is the dth diagonal entry of $\mathbf{X}$, and the (q_1,q_2)th entries of $\mathbf{M}^d_{\boldsymbol{\nu},\boldsymbol{\nu}}$,

$\mathbf{M}^d_{\boldsymbol{\nu},\boldsymbol{\tau}}$, and $\mathbf{M}^d_{\boldsymbol{\tau},\boldsymbol{\tau}}$, $q_1, q_2 \in \{1,\cdots,Q\}$, are $\alpha^H_{q_1}\alpha_{q_2}\boldsymbol{\Psi}'(d,q_1)^H\boldsymbol{\Psi}'(d,q_2)$, $\alpha^H_{q_1}\alpha_{q_2}\boldsymbol{\Psi}'(d,q_1)^H\boldsymbol{\Psi}''(d,q_2)$, and $\alpha^H_{q_1}\alpha_{q_2}\boldsymbol{\Psi}''(d,q_1)^H\boldsymbol{\Psi}''(d,q_2)$, respectively.

Observing the expression of $\boldsymbol{\Psi}'$ and $\boldsymbol{\Psi}''$ in (37) and (38), we find that the diagonal entries of $\mathbf{M}^d_{\boldsymbol{\nu},\boldsymbol{\nu}}$, $\mathbf{M}^d_{\boldsymbol{\tau},\boldsymbol{\tau}}$, and $\mathbf{M}^d_{\boldsymbol{\nu},\boldsymbol{\tau}}$ are $|\alpha_q|^2(\lfloor d/G\rfloor-1)^2$, $|\alpha_q|^2\mathrm{mod}^2(d,G)$, and $|\alpha_q|^2\mathrm{mod}(d-1,G)(\lfloor d/G\rfloor-1)$, respectively, with $q\in\{1,\cdots,Q\}$. The non-diagonal entries of $\mathbf{M}^d_{\boldsymbol{\nu},\boldsymbol{\nu}}$, $\mathbf{M}^d_{\boldsymbol{\tau},\boldsymbol{\tau}}$, and $\mathbf{M}^d_{\boldsymbol{\nu},\boldsymbol{\tau}}$ have linearly increasing phase shifts. Since M and G are sufficiently large, the summation from $d=1$ to $d=MG$ would make the non-diagonal entries have far lower amplitude than the diagonal entries. We define $\tilde{m}(d)=(\lfloor d/G\rfloor-1)$ and $\tilde{g}(d)=\mathrm{mod}(d-1,G)$ and rewrite (27) as

$$\begin{aligned}\mathbf{F}^r_{\psi} =&2\sigma^{-2}\mathrm{Re}\left\{\sum_{d=1}^{MG}x_d\begin{bmatrix}\tilde{m}(d)^2\mathbf{N}^d_{\boldsymbol{\nu},\boldsymbol{\nu}} & \tilde{m}(d)\tilde{g}(d)\mathbf{N}^d_{\boldsymbol{\nu},\boldsymbol{\tau}}\\ \tilde{g}(d)\tilde{m}(d)\mathbf{N}^d_{\boldsymbol{\tau},\boldsymbol{\nu}} & \tilde{g}(d)^2\mathbf{N}^d_{\boldsymbol{\tau},\boldsymbol{\tau}}\end{bmatrix}\right\}\\ \approx&2\sigma^{-2}\mathrm{Re}\left\{\sum_{d=1}^{MG}x_d\begin{bmatrix}\tilde{m}(d)^2\boldsymbol{\Lambda}^2 & \tilde{m}(d)\tilde{g}(d)\boldsymbol{\Lambda}^2\\ \tilde{g}(d)\tilde{m}(d)\boldsymbol{\Lambda}^2 & \tilde{g}(d)^2\boldsymbol{\Lambda}^2\end{bmatrix}\right\},\end{aligned} \tag{28}$$

where $\tilde{m}(d)^2\mathbf{N}^d_{\boldsymbol{\nu},\boldsymbol{\nu}}=\mathbf{M}^d_{\boldsymbol{\nu},\boldsymbol{\nu}}$, $\tilde{m}(d)\tilde{g}(d)\mathbf{N}^d_{\boldsymbol{\nu},\boldsymbol{\tau}}=\mathbf{M}^d_{\boldsymbol{\nu},\boldsymbol{\tau}}$, and $\tilde{g}(d)^2\mathbf{N}^d_{\boldsymbol{\tau},\boldsymbol{\tau}}=\mathbf{M}^d_{\boldsymbol{\tau},\boldsymbol{\tau}}$. Then, optimizing the FIM is equivalent to optimizing

$$\begin{aligned}\mathbf{F}_{\mathrm{eig}} &= 2\sigma^{-2}\mathrm{Re}\left\{\sum_{d=1}^{MG}x_d\begin{bmatrix}\tilde{m}(d)^2 & \tilde{m}(d)\tilde{g}(d)\\ \tilde{g}(d)\tilde{m}(d) & \tilde{g}(d)^2\end{bmatrix}\otimes\boldsymbol{\Lambda}^2\right\}\\ &= 2\sigma^{-2}\mathrm{Re}\left\{\sum_{m=0}^{M-1}\sum_{g=0}^{G-1}x_d\begin{bmatrix}m^2 & mg\\ gm & g^2\end{bmatrix}\otimes\boldsymbol{\Lambda}^2\right\}.\end{aligned} \tag{29}$$

The closed-form solution will be obtained by maximizing the minimum eigenvalue of $\mathbf{F}_{\mathrm{eig}}$. □

Remark 1: From the derivations of Theorem 1, we can approximately analyze the impacts of Q or L on the CRB. Referring to the expression of $\mathbf{F}_{\mathrm{eig}}$, with a given number of M and G, a larger dimension of $\boldsymbol{\Lambda}^2$, i.e., $L+1$, not only increases the number of diagonal entries of $\mathbf{F}_{\mathrm{eig}}$ but also leads to the increase of non-diagonal entries. Hence, the eigenvalues of $\mathbf{F}_{\mathrm{eig}}$ would either increase or decrease with L increasing. In fact, we find that with L increasing, the CRB of $\mathbf{F}_{\mathrm{eig}}$ increases accordingly, which is as expected, since a larger L means that there are more parameters to be estimated in the same FT resources. These relationships can be observed from the numerical results shown in Fig. 2.

2) Radar CRB of multi-user system: We derive the radar CRB of multi-user system by exploiting the relationship of multiple UEs' parameters. Recall that the number of independent parameters is Q which is less than LU. The parameters of interest are stacked into a $3Q\times 1$ real-valued vector, i.e., $[\boldsymbol{\nu}^T,\boldsymbol{\tau}^T,\boldsymbol{\omega}^T]^T$ with $\boldsymbol{\nu}=[\nu_1,\cdots,\nu_Q]^T$, $\boldsymbol{\tau}=[\tau_1,\cdots,\tau_Q]^T$, and $\boldsymbol{\omega}=[\omega_1,\cdots,\omega_Q]^T$. Since the parameters become independent to the UEs, the CRB derivations are the same as those in single-user systems. Hence, the signal transmitted by multiple UEs can be seen as a whole sensing signal of a single transmitter.

Similar to the single-user system, we stack the measurements of $y_n[g,m]$ from $[g,m]=[0,0]$ to $[g,m]=[G-1,M-1]$ into an $MG\times 1$ vector,

$$\begin{aligned}\mathbf{y}_n =&[y_n[0,0],\cdots,y_n[G-1,0],\cdots,y_n[G-1,M-1]]^T\\ =&\sum_{u=1}^{U}\sum_{l=1}^{L}\alpha_{l,u}e^{jn\omega_{l,u}}\boldsymbol{\psi}(\nu_{l,u},\tau_{l,u})\circ\mathbf{r}\circ\boldsymbol{\delta}_q\\ &+\sum_{u=1}^{U}\alpha_{0,u}e^{jn\omega_{0,u}}\boldsymbol{\psi}(\nu_{0,u},\tau_{0,u})\circ\mathbf{r}\circ\boldsymbol{\delta}_q+\mathbf{z}_n\\ =&\sum_{q=1}^{Q}\alpha_q e^{jn\omega_q}\boldsymbol{\psi}(\nu_q,\tau_q)\circ\mathbf{r}\circ\boldsymbol{\delta}_q+\mathbf{i}_n+\mathbf{z}_n,\end{aligned} \tag{30}$$

where α_q is the sum of $\alpha_{l,u}$ of which path reflected by the same object, τ_q, ν_q, and ω_q are the mean delay, Doppler shift, and AoA between the object and BS, the entries of $\boldsymbol{\delta}_q$ are either 1 or 0 with 1 indicating that the signal in the (g,m)-th FT bin impinges on the qth object, $\boldsymbol{\psi}(\nu_q,\tau_q)$ is given by (7), $\mathbf{i}_n$ is the interference vector, and $\mathbf{z}_n$ is the noise vector. With replacing by $\boldsymbol{\psi}(\nu_l,\tau_l)$ of the single-user systems by $\boldsymbol{\psi}(\nu_q,\tau_q)\circ\boldsymbol{\delta}_q$, the received signal vector has the same form as (18). We omit the following FIM derivations and optimizations for multi-user systems as they are the same as those for single-user systems.

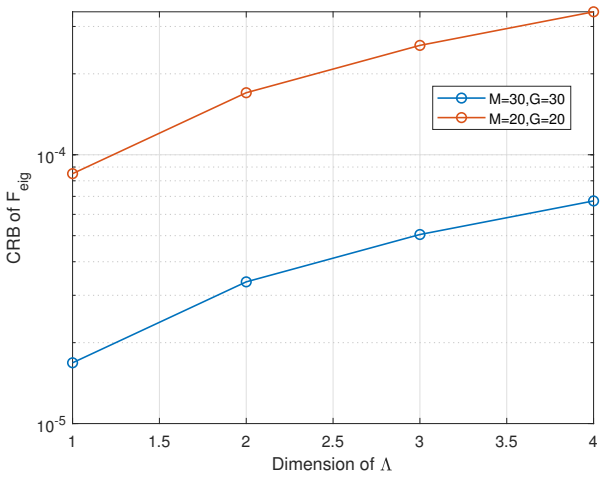

Fig. 2. Illustration of L on CRB using the closed-form $\mathbf{F}_{\mathrm{eig}}$. Here, we let $\boldsymbol{\Lambda}=\mathbf{I}$ of which dimension equals $L+1$. The y-label is the corresponding CRB that is given by $\mathrm{Tr}(\mathbf{F}^{-1}_{\mathrm{eig}})$.

C. ISAC FT-Bin Optimizations

In this subsection, we leverage the previously derived radar and communication FIMs (CRBs) to formulate two FT-bin optimization problems that strike a balance between radar and communication performance.

The previously derived communication CRB has two distinct outcomes depending on whether the channel coefficients are i.i.d or not. For correlated channel coefficients, which indicates the number of paths is small, both the radar and communication CRB matrices prioritize the accuracy of parameters, albeit with slightly differing forms. Conversely, with a large L, the communication CRB can shift its focus to ensuring the accuracy of all channel coefficients. The optimal communication

matrix is similar to an identity matrix, diverging significantly from the optimization outcome of radar CRB minimization. Consequently, the approach to formulating an ISAC problem must vary based on the form of the communication CRB (FIM). We articulate two distinct ISAC problems as follows.

When the communication FIM is derived w.r.t. channel coefficients, we can formulate the ISAC optimization problem as

$$\begin{aligned}&\mathbf{x}^\star = \arg\min_{\mathbf{x}} \max_{\boldsymbol{\epsilon}^u} (-t_u)\\ &\text{s.t.} \quad \mathbf{F}_c^u \succeq t_u, \mathbf{F}_{\boldsymbol{\omega},\boldsymbol{\omega}}^r \succeq t_\omega \mathbf{I}, \mathbf{F}_\psi^r \succeq t\mathbf{I}, \|\mathbf{x}\|_F^2 \le P_o U. \end{aligned} \tag{31}$$

Note that t and t_ω are thresholds for delay-Dopplers and AoAs, respectively, which can control the radar CRB. On the other hand, t_u that is dependent on each UE can minimize the communication CRB. The optimization problem above is dependent on the UE allocation vector, $\boldsymbol{\epsilon}^u$, which makes the joint problem difficult to solve. Additionally, from the following simulation results in Section IV, we note that the optimal radar FT bins have sparse properties while the optimal communication FT bins should occupy all of MG bins evenly. This indicates that the optimal communication and radar FT bins do not interfere with each other much. Hence, we can use a weighted sum of two individually optimal FT bins as a suboptimal solution that achieves a good balance between performance and complexity. Hence, we formulate the ISAC FT bin as

$$\mathbf{x} = \mu \mathbf{r}^\star + (1-\mu)\mathbf{c}^\star, \tag{32}$$

where $\mathbf{r}^\star$ is the optimal radar FT bin, $\mathbf{c}^\star$ is the optimal communication FT bin, and μ is a weighting factor.

When the communication CRB is derived w.r.t. parameters, it is essential to possess all the parameters for reconstructing the communication channel. In contrast, the radar only requires part of parameters dependent on the objects. To enhance the accuracy of parameter sensing, a collective processing approach can be adopted for signals from all UEs, as discussed in Section III-B. Notably, communication can utilize radar parameters for reconstructing the communication channel, given their equivalence. However, the individual path gains of each UE cannot be shared. We can formulate the ISAC problem, akin to (24), with the FIM of path gains being UE-dependent. The optimization problem is thus formulated as follows:

$$\begin{aligned}&\mathbf{x}^\star = \arg\min_{\mathbf{x}} \quad -t\\ &\text{s.t.} \quad \mathbf{F}_\psi \succeq t\mathbf{I}, \mathbf{F}_{\boldsymbol{\omega},\boldsymbol{\omega}} \succeq t_\omega \mathbf{I}, \mathbf{F}_{\boldsymbol{\alpha},\boldsymbol{\alpha}} \succeq t_\alpha \mathbf{I}, \|\mathbf{x}\|_F^2 \le P_o U. \end{aligned} \tag{33}$$

For the problem above, the FIMs of delays, AoAs, and Dopplers are derived w.r.t. the objects instead of paths, and their expressions are the same as those in Appendix A and B by replacing L with Q. The FIM of path gains is the same as the one in (17). The problem above can be solved in the same way as in (17) using the convex toolboxes.

IV. Simulation Results

In this section, we provide simulation results to validate the proposed scheme, using numerical experiments on MATLAB. Unless mentioned specifically, all the parameters are the same as follows. We simulate an ISAC uplink system where a BS receives signals from $U = 2$ UEs each having an NLOS channel with $L = 2$ paths that are generated by radio-silent $Q = 3$ objects. We assume that the objects are far from the BS, such that the delays between an object and different UEs are nearly the same. Each UE has a transmit power of $P_o = 3$ W. The carrier frequency is 3 GHz. The frequency bandwidth is 128 MHz and the number of subcarriers is $G = 32$. Hence, the OFDM symbol period T is 0.25 μs. The delay of each path is a random value ranging from 0 to $T/2$. The length of CP is $D = 16$ to avoid inter-symbol interference. The interval between two packets, T', is 1 ms. We use the OFDM pilot symbols in $M = 30$ time slots for sensing parameter estimation. The velocities of objects range from -30 meter-per-second (mps) to 30 mps, and the Doppler frequency is randomly distributed over $[-0.3, 0.3]$ kHz. The path gains yield a complex Gaussian distribution, $\mathcal{CN}(0,1)$. We consider a single-antenna system for convenience and thus the angle parameters can be discarded.

A. Single-user Cases

Fig. 3 plots the CRB of radar sensing and communications using different FT bins, including the optimal radar one, the optimal communication one that is equivalent to binary phase shift keying (BPSK), 8- and 16-quadrature amplitude modulation (QAM) signals, and a benchmark solution in [22]. Since only the magnitude of constellations affects the CRB, we align the magnitude of constellations of 8- and 16-QAM in sequential order. For example, the 8-QAM has the power allocations of $[1, 2, \cdots, 1, 2]$ since there are only two types of magnitudes for 8-QAM. All schemes have the same power constraint of 3 W. The x-label is the SNR, defined as P_o/σ^2. The CRB of radar is calculated as $\mathrm{Tr}(\mathbf{F}_r^{-1})$ and the CRB of communication is derived w.r.t. parameters, i.e., $\mathrm{Tr}((\mathbf{F}_c^A)^{-1})$. From Fig. 3 (a), we see that the proposed radar FT bin achieves the lowest radar CRB. The optimal communication FT bin (BPSK) achieves the highest CRB compared with other FT allocation solutions, which is as expected because according to Corollary 1, the optimal radar FT bin should have a limited number of non-zero entries. The gap between the two solutions can be as large as 10 dB. The 8-QAM and 16-QAM achieve nearly the same CRB as the BPSK. The uneven FT amplitudes of 8-QAM and 16-QAM signals lead to slightly lower radar CRB compared with the BPSK. The benchmark solution in [22] achieves higher CRB compared with our scheme.

Fig. 3 (b) plots the CRB of communication using the optimal communication FT bin and the benchmarks. We can see that the optimal communication FT bin (BPSK) achieves the lowest CRB of communication and the other QAM signals have slightly higher CRBs. The optimal radar FT bin achieves a much higher CRB since the radar CRB minimizations do not take the path gains into account but the communication CRB includes the path gains. Note that the optimal radar FT

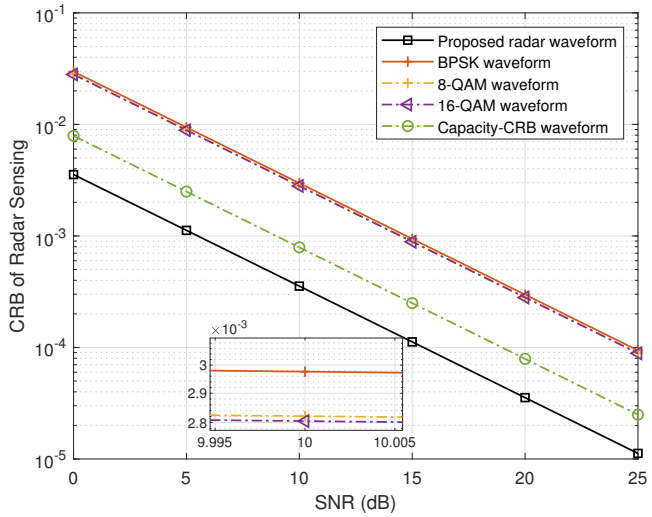

(a) Radar CRB

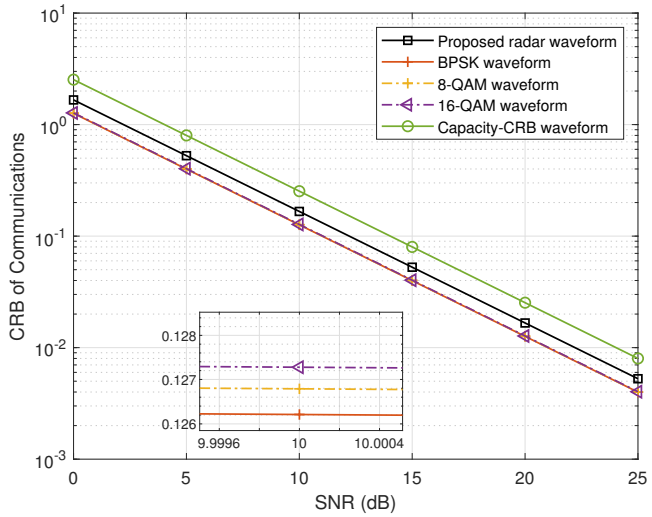

(b) Communication CRB

Fig. 3. Performances of Radar and Communication CRB using the proposed and benchmark FT bins.

bins show a sparse property while the optimal communication ones should have evenly distributed power on all FT bins.

Fig. 4 illustrates the impacts of the ISAC weighting factor, μ, on the radar and communication CRBs. The SNR is fixed as 0 dB. When μ increases from 0 to 1, we see that the radar CRB decreases from 1.4×10^{-2} to 5×10^{-3}. This means that, when using the optimal communication waveform for radar sensing, the increase of CRB (performance degradation) is about 9×10^{-3}. On the other hand, the communication CRB increases from about 1.4 to 1.8. The gap is nearly 0.4 that is much larger than 9×10^{-3}. This is because the communication CRB is additionally affected by the estimation error of path gains, besides delays and Dopplers. The ideal ISAC FT bins should achieve the optimal CRB no matter how large the μ is. The ISAC optimization performance can be evaluated by measuring the gap between the ISAC CRB curve and the ideal one.

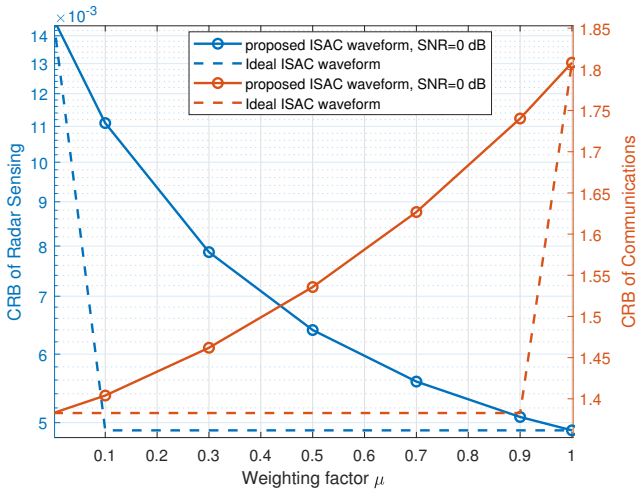

Fig. 4. Impacts of the ISAC weighting factor, μ, on Radar and Communication CRB.

Fig. 5 plots the CRBs of radar and communication versus SNR and the number of paths/objects using the optimal communication FT bins. Both CRBs have a linear relationship with the SNR. We let L vary from 3 to 10 and assume that the communication channel is i.i.d in the FT bins. Recall that we derived two types of CRBs for communications: one for the correlated channel coefficients and the other for i.i.d channel coefficients. Here, the number of paths is large enough to guarantee i.i.d. channel coefficients and thus we use the CRB w.r.t. channel coefficients for communications. For radar, we use the CRB w.r.t. parameters. It is noted that $L = Q$ for the single-user cases, which means that the radar CRB is similar to the communication CRB w.r.t. parameters. Fig. 5 (a) shows that the radar CRB rises with L increasing, which is because there are more parameters to be estimated in the same FT bins. Fig. 5 (b) shows that the communication CRB drops with L increasing, which is because the total number of channel coefficients is unchanged with L increasing but the channel gain is enhanced. Another meaningful outcome is that the communication CRB is much larger than the radar CRB. At the same SNR, the radar CRB is about 20 dB lower than the communication CRB and the gap narrows with L increasing. This is because the communication CRB measures the errors of $MG = 960$ channel coefficients in total and each coefficient only has one measurement, whereas the radar CRB only counts in the error of $L \times 2$ parameters and each parameter has 960 measurements. This indicates that the parameter estimators are preferable ways to rebuild the channel.

B. Multi-user Cases

Now, in this subsection, we begin to allocate the FT bins to multi-users and analyze the CRB achieved by different allocations.

Fig. 6 shows the CRB of communications versus U and L. The SNR is fixed at 0 dB. The number of objects is either $L = 2$ or $L = 10$ to simulate a dependent or an independent channel, respectively. The parameters among

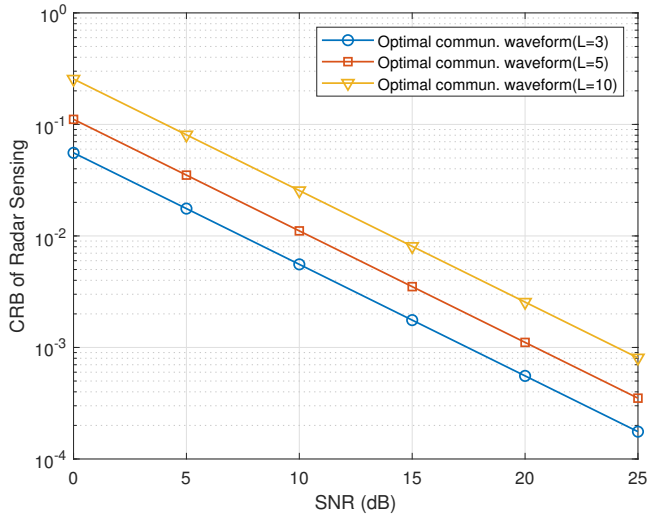

(a) Radar CRB

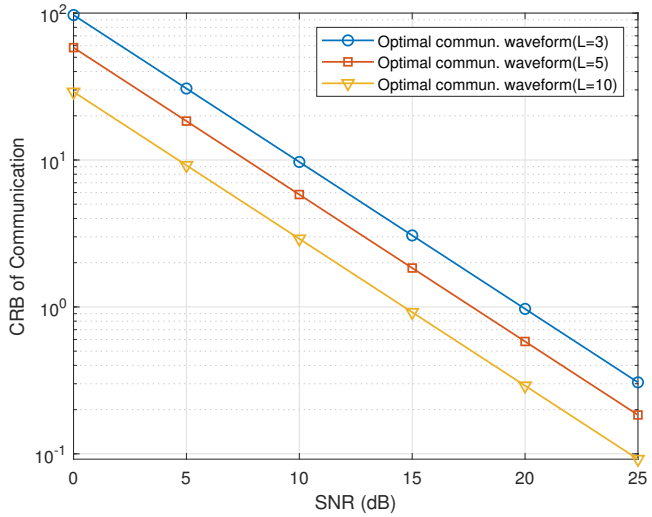

(b) Communication CRB

Fig. 5. Impacts of L on Radar and Communication CRB.

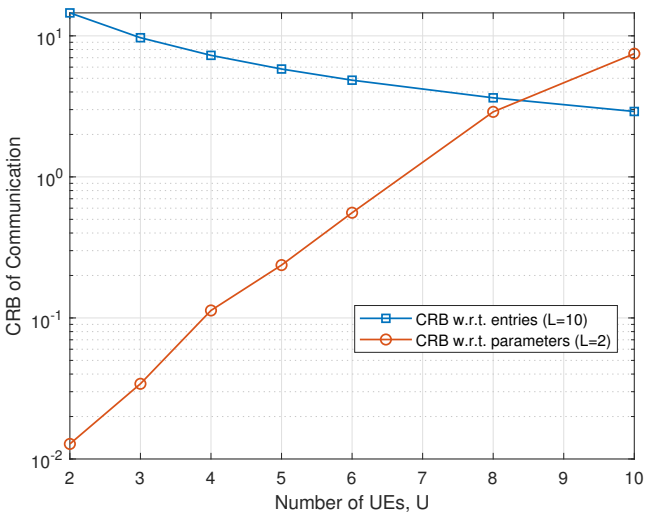

Fig. 6. Communication CRB comparisons under different U and L.

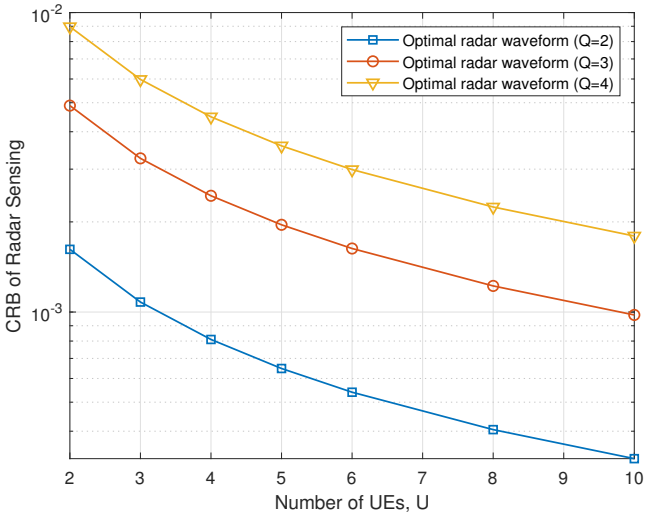

Fig. 7. Radar CRB comparisons under different U and Q.

different UEs are not related to one another, that is, $Q = LU$. We adopt an interleaved time-domain allocation, where each UE occupies an interleaved segment of time slots from $m = 0$ to $m = 29$. Hence, the parameters can be given by τ and $U\nu$. From the figure, we see that the communication CRB w.r.t. channel coefficients decreases with U increasing, which is because each UE has the same transmit power and the increase of U makes the received power increase accordingly. The communication CRB w.r.t. parameters shows an opposite trend to its counterpart and linearly increases with U increasing. This indicates that, with U increasing, each UE has a smaller number of FT bins to estimate the parameters of interest. Even though more UEs bring higher received power, the reduction of FT bins has a significant impact on the estimation accuracy of parameters. When $U = 8$, we see that the CRB w.r.t. parameters begins to exceed the CRB w.r.t. channel coefficients. When the Doppler shifts are all zeros in a static channel, the CRB w.r.t. parameters would be related to delays only. When adopting interleaved frequency-domain allocation, where each UE occupies an interleaved segment of frequencies from $g = 0$ to $g = 31$, the CRB w.r.t. delays will be affected but the CRB w.r.t. Doppler shifts will be unaffected.

Fig. 7 depicts the CRB of radar versus U and Q. The other setups are the same as those in Fig. 6. From the figure, we see that when the number of UEs increases, the CRB of radar drops, and the drop rate declines. Note that the radar CRB uses all FT bins to estimate the parameters of objects. Hence, the case here becomes similar to the one in Fig. 5. The difference is that here the adopted FT bin is the optimal radar one. With L increases, we observe that the radar CRB increases too, which is as expected since more parameters need to be estimated.

Fig. 8 unfolds the impact of a LOS path on the CRB of radar and communication. The power of the LOS path is 10 dB higher than that of NLOS paths. We adopt an interleaved

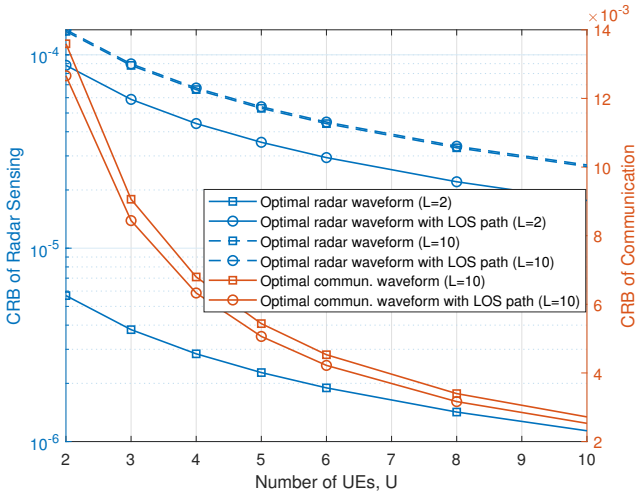

Fig. 8. Impacts of the LOS path on CRBs under different U and L.

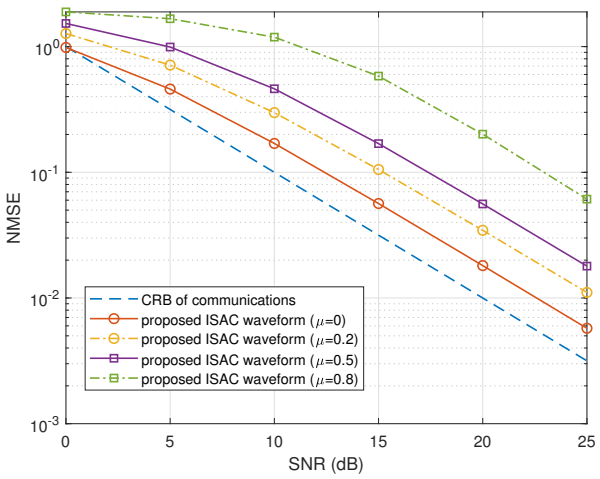

Fig. 9. NMSE of communication channels using the proposed ISAC FT-bin allocations and the MMSE estimator.

time-domain allocation. The radar FIM after adding the LOS path is (21), where we assume the Doppler shift and delay of each UE's LOS path are known by BS and we estimate $\alpha_{u,0}$ as $\text{mean}(|y_n[g,m]|\epsilon_u^{g,m})\exp(j\angle(y_n[0,m_u]))$ with m_u the beginning index of each UE. By adding a LOS path to the channel, we can see that radar achieves higher CRB. When $L=2$, the increase of radar CRB is significant, which means that the LOS path has a strong interference with the estimation of parameters. When $L=10$, we see that the CRB of radar is nearly unaffected by the LOS path as the dominant power of the LOS path has been removed in (21). As for the communication, when $L=10$, we can see that the communication CRB drops slightly after adding the LOS path impacts.

In Fig. 9, we plot the normalized mean squared error (NMSE) of channel estimations, i.e., $\sum_{u=1}^{U}\|\mathbf{h}^u-\hat{\mathbf{h}}^u\|_F^2/\|\mathbf{h}^u\|_F^2$, where $\hat{\mathbf{h}}^u$ is the estimated channel entries using the traditional minimum mean squared error (MMSE) estimator. We let U and L be 2 and 3, respectively. Hence,

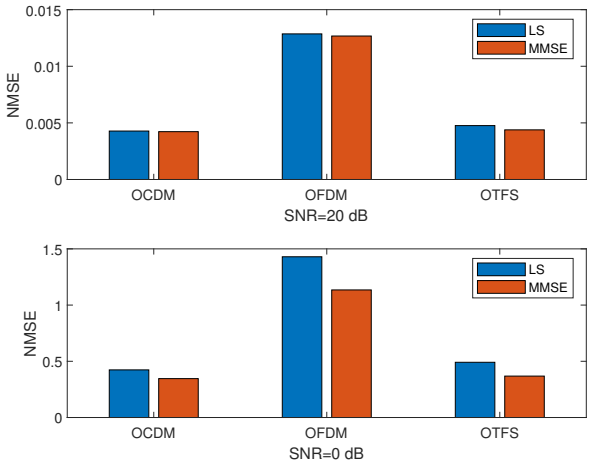

Fig. 10. NMSE of channel estimates using different FT waveforms.

the CRB is derived w.r.t. channel coefficients. For the FT resource allocations of $\mathbf{x}$, we adopt our proposed weighted-sum ISAC FT bins. It is seen that when using the optimal communication waveform, i.e., $\mu=0$, the actually achieved NMSE approaches to the CRB of communications. With μ increasing, the achieved NMSE of communications increases.

We also compare systems with different FT waveforms, via the performance metric of NMSE of channel estimates, as shown in Fig. 10. We consider a single-user ISAC uplink system with $L=3$ channel taps. The number of subcarriers is $G=64$ and the number of symbols is $M=100$. Other parameters are the same with those used in generating Fig. 9. We primarily compare the OFDM waveform with two recently proposed waveforms: orthogonal-time-frequency-space (OTFS) and orthogonal-chirp-division-multiplexing (OCDM) signals. The generalized-adaptive-spreading-modulation (GASM) proposed in [29] is a generalized form of OCDM; hence, its performance should be similar to that of OCDM. We note that, for all the waveforms, the received signals can be expressed in the form $\mathbf{Y}=\mathbf{HX}+\mathbf{N}$ in different domains, where $\mathbf{H}$ is the channel matrix, $\mathbf{X}$ is the pilot signal, and $\mathbf{N}$ is the AWGN. The channel estimation is obtained via least-square (LS) and minimum-mean-squared-error (MMSE) methods. From the figure, we observe that OCDM and OTFS achieve nearly the same NMSE, which is about one-third of that of OFDM. The results demonstrate that OCDM and OTFS lead to lower channel estimation errors and potentially lower CRBs. However, their CRBs are yet to be derived. Our work proposed in this paper may be extended to systems with these waveforms after deriving the CRB metrics.

V. Conclusions

In this paper, we have undertaken the CRB derivations and optimizations tailored for uplink ISAC systems. Specifically, communication CRBs are derived with respect to both channel coefficients and sensing parameters. The radar CRB, on the other hand, consolidates information from all FT bins to estimate object parameters. Theoretical and simulation results

jointly reveal a distinctive pattern: the radar CRB induces sparsity in the FT-domain resource, while the communication CRB of channel coefficients exhibits a more uniform FT distribution. Capitalizing on this observation, we formulated an ISAC FT resource optimization problem and solved it using weighted-sum solutions. The CRB demonstrates a linear decrease with increasing SNR. When allocating multiple UEs on FT resources, interleaved time-domain allocations outperform interleaved frequency-domain allocations. For a certain amount of objects, both the radar and communication CRBs experience a decrease with the growing number of UEs. In essence, the amalgamation of measurements from multiple UEs improves estimation accuracy for both radar and communication systems.

Appendix A
Subblocks of FIM w.r.t. Delay, Doppler, and AoA

Note that the FIMs are constructed by the derivatives w.r.t. each group of parameters. Referring to (14), we have

$$D_{\boldsymbol{\nu}}(\mathbf{g}) = \frac{\partial \mathbf{g}}{\partial \boldsymbol{\nu}} = \mathrm{diag}(\mathbf{1}_N \otimes \mathbf{x})\mathbf{A} \odot \boldsymbol{\Psi}'\boldsymbol{\Lambda}, \tag{34}$$

$$D_{\boldsymbol{\tau}}(\mathbf{g}) = \frac{\partial \mathbf{g}}{\partial \boldsymbol{\tau}} = \mathrm{diag}(\mathbf{1}_N \otimes \mathbf{x})\mathbf{A} \odot \boldsymbol{\Psi}''\boldsymbol{\Lambda}, \tag{35}$$

$$D_{\boldsymbol{\omega}}(\mathbf{g}) = \frac{\partial \mathbf{g}}{\partial \boldsymbol{\omega}} = \mathrm{diag}(\mathbf{1}_N \otimes \mathbf{x})\dot{\mathbf{A}} \odot \boldsymbol{\Psi}\boldsymbol{\Lambda}, \tag{36}$$

where $\boldsymbol{\Lambda} = \mathrm{diag}\,(\alpha_0, \cdots, \alpha_L)$, $\mathbf{A} = [\mathbf{a}(\omega_0), \cdots, \mathbf{a}(\omega_L)]$, $\boldsymbol{\Psi} = [\boldsymbol{\psi}(\nu_0, \tau_0), \cdots, \boldsymbol{\psi}(\nu_L, \tau_L)]$,

$$\boldsymbol{\Psi}' = \left[\frac{\partial \boldsymbol{\psi}(\nu_0, \tau_0)}{\partial V\nu_0}, \cdots, \frac{\partial \boldsymbol{\psi}(\nu_L, \tau_L)}{\partial V\nu_L}\right], \tag{37}$$

$$\boldsymbol{\Psi}'' = \left[\frac{\partial \boldsymbol{\psi}(\nu_0, \tau_0)}{\partial \tau_0/T}, \cdots, \frac{\partial \boldsymbol{\psi}(\nu_L, \tau_L)}{\partial \tau_L/T}\right], \tag{38}$$

$$\dot{\mathbf{A}} = \left[\frac{\partial \mathbf{a}(\omega_0)}{\partial \omega_0}, \cdots, \frac{\partial \mathbf{a}(\omega_L)}{\partial \omega_L}\right], \tag{39}$$

and $\mathbf{x}$ is the ISAC FT bin. For communication only, we let $\mathbf{x} = \mathbf{c}$. For radar only, we let $\mathbf{x} = \mathbf{r}$. It should be highlighted that, for communications, the index should be (l, u) that varies from $(l, u) = (0, 1)$ to $(l, u) = (L, U)$, while for radar, the index varies from $l = 1$ to $l = Q$.

For each subblock of FIM, denoting $\mathbf{X} = \mathrm{diag}(\mathbf{x})^2$, we have

$$\begin{aligned}\mathbf{F}_{\boldsymbol{\nu},\boldsymbol{\nu}} &= 2\sigma^{-2}\mathrm{Re}\{D_{\boldsymbol{\nu}}(\mathbf{g})^H D_{\boldsymbol{\nu}}(\mathbf{g})\} \\ &= 2\sigma^{-2}\mathrm{Re}\{(\boldsymbol{\Lambda}\mathbf{A} \odot \boldsymbol{\Psi}')^H \mathbf{I}_N \otimes \mathbf{X}(\boldsymbol{\Lambda}\mathbf{A} \odot \boldsymbol{\Psi}')\} \\ &= 2\sigma^{-2}\boldsymbol{\Lambda}^H\mathrm{Re}\{(\mathbf{A} \odot \boldsymbol{\Psi}')^H \mathbf{I}_N \otimes \mathbf{X}(\mathbf{A} \odot \boldsymbol{\Psi}')\}\boldsymbol{\Lambda},\end{aligned} \tag{40}$$

$$\mathbf{F}_{\boldsymbol{\tau},\boldsymbol{\tau}} = 2\sigma^{-2}\boldsymbol{\Lambda}^H\mathrm{Re}\{(\mathbf{A} \odot \boldsymbol{\Psi}'')^H \mathbf{I}_N \otimes \mathbf{X}(\mathbf{A} \odot \boldsymbol{\Psi}'')\}\boldsymbol{\Lambda}, \tag{41}$$

$$\mathbf{F}_{\boldsymbol{\omega},\boldsymbol{\omega}} = 2\sigma^{-2}\boldsymbol{\Lambda}^H\mathrm{Re}\{(\dot{\mathbf{A}} \odot \boldsymbol{\Psi})^H \mathbf{I}_N \otimes \mathbf{X}(\dot{\mathbf{A}} \odot \boldsymbol{\Psi})\}\boldsymbol{\Lambda}, \tag{42}$$

$$\mathbf{F}_{\boldsymbol{\nu},\boldsymbol{\omega}} = 2\sigma^{-2}\boldsymbol{\Lambda}^H\mathrm{Re}\{(\mathbf{A} \odot \boldsymbol{\Psi}')^H \mathbf{I}_N \otimes \mathbf{X}(\dot{\mathbf{A}} \odot \boldsymbol{\Psi})\}\boldsymbol{\Lambda}, \tag{43}$$

$$\mathbf{F}_{\boldsymbol{\nu},\boldsymbol{\tau}} = 2\sigma^{-2}\boldsymbol{\Lambda}^H\mathrm{Re}\{(\mathbf{A} \odot \boldsymbol{\Psi}')^H \mathbf{I}_N \otimes \mathbf{X}(\mathbf{A} \odot \boldsymbol{\Psi}'')\}\boldsymbol{\Lambda}, \tag{44}$$

$$\mathbf{F}_{\boldsymbol{\tau},\boldsymbol{\omega}} = 2\sigma^{-2}\boldsymbol{\Lambda}^H\mathrm{Re}\{(\mathbf{A} \odot \boldsymbol{\Psi}'')^H \mathbf{I}_N \otimes \mathbf{X}(\dot{\mathbf{A}} \odot \boldsymbol{\Psi})\}\boldsymbol{\Lambda}. \tag{45}$$

Note that $\mathbf{F}_{\boldsymbol{\omega},\boldsymbol{\tau}} = \mathbf{F}_{\boldsymbol{\tau},\boldsymbol{\omega}}^H$, $\mathbf{F}_{\boldsymbol{\tau},\boldsymbol{\nu}} = \mathbf{F}_{\boldsymbol{\nu},\boldsymbol{\tau}}^H$, and $\mathbf{F}_{\boldsymbol{\omega},\boldsymbol{\nu}} = \mathbf{F}_{\boldsymbol{\nu},\boldsymbol{\omega}}^H$.

Appendix B
Subblocks of FIM w.r.t. Path Gains

Note that the FIM are constructed by the derivatives w.r.t. each kind of parameter. Referring to (14), we define

$$D_{\boldsymbol{\alpha}}(\mathbf{g}) = \left[\frac{\partial \mathbf{g}}{\partial \mathrm{Re}\{\boldsymbol{\alpha}\}}, \frac{\partial \mathbf{g}}{\partial \mathrm{Im}\{\boldsymbol{\alpha}\}}\right] = [1, j] \otimes (\mathbf{A} \odot \boldsymbol{\Psi}\dot{\boldsymbol{\Lambda}}), \tag{46}$$

with

$$\dot{\boldsymbol{\Lambda}} = \left[\frac{\partial \boldsymbol{\alpha}}{\partial \alpha_0}, \cdots, \frac{\partial \boldsymbol{\alpha}}{\partial \alpha_L}\right] = \mathbf{I}. \tag{47}$$

The subblock of FIM w.r.t. $\boldsymbol{\alpha}$ is

$$\begin{aligned}\mathbf{F}_{\boldsymbol{\alpha},\boldsymbol{\alpha}} &= 2\sigma^{-2}\mathrm{Re}\{D_{\boldsymbol{\alpha}}(\mathbf{g})^H D_{\boldsymbol{\alpha}}(\mathbf{g})\} \\ &= 2\sigma^{-2}\mathrm{Re}\left\{\begin{bmatrix} 1 & -j \\ j & 1 \end{bmatrix} \otimes \left((\mathbf{A} \odot \boldsymbol{\Psi})^H \mathbf{I}_N \otimes \mathbf{X}(\mathbf{A} \odot \boldsymbol{\Psi})\right)\right\}.\end{aligned} \tag{48}$$

The subblock of FIM w.r.t. $\boldsymbol{\alpha}$ and $\boldsymbol{\tau}$ is

$$\begin{aligned}\mathbf{F}_{\boldsymbol{\alpha},\boldsymbol{\tau}} &= 2\sigma^{-2}\mathrm{Re}\{D_{\boldsymbol{\alpha}}(\mathbf{g})^H D_{\boldsymbol{\tau}}(\mathbf{h})\} \\ &= 2\sigma^{-2}\mathrm{Re}\{[1, j]^H \otimes (\mathbf{A} \odot \boldsymbol{\Psi})^H \mathbf{I}_N \otimes \mathbf{X}(\mathbf{A} \odot \boldsymbol{\Psi}''\boldsymbol{\Lambda})\}.\end{aligned} \tag{49}$$

The subblock of FIM w.r.t. $\boldsymbol{\alpha}$ and $\boldsymbol{\nu}$ is

$$\begin{aligned}\mathbf{F}_{\boldsymbol{\alpha},\boldsymbol{\nu}} &= 2\sigma^{-2}\mathrm{Re}\{D_{\boldsymbol{\alpha}}(\mathbf{g})^H D_{\boldsymbol{\nu}}(\mathbf{h})\} \\ &= 2\sigma^{-2}\mathrm{Re}\{[1, j]^H \otimes (\mathbf{A} \odot \boldsymbol{\Psi})^H \mathbf{I}_N \otimes \mathbf{X}(\mathbf{A} \odot \boldsymbol{\Psi}'\boldsymbol{\Lambda})\}.\end{aligned} \tag{50}$$

The subblock of FIM w.r.t. $\boldsymbol{\alpha}$ and $\boldsymbol{\omega}$ is

$$\begin{aligned}\mathbf{F}_{\boldsymbol{\alpha},\boldsymbol{\omega}} &= 2\sigma^{-2}\mathrm{Re}\{D_{\boldsymbol{\alpha}}(\mathbf{h})^H D_{\boldsymbol{\omega}}(\mathbf{h})\} \\ &= 2\sigma^{-2}\mathrm{Re}\{[1, j]^H \otimes (\mathbf{A} \odot \boldsymbol{\Psi})^H \mathbf{I}_N \otimes \mathbf{X}(\dot{\mathbf{A}} \odot \boldsymbol{\Psi}\boldsymbol{\Lambda})\}.\end{aligned} \tag{51}$$

Note that $\mathbf{F}_{\boldsymbol{\alpha},\boldsymbol{\tau}} = \mathbf{F}_{\boldsymbol{\tau},\boldsymbol{\alpha}}^H$, $\mathbf{F}_{\boldsymbol{\alpha},\boldsymbol{\nu}} = \mathbf{F}_{\boldsymbol{\nu},\boldsymbol{\alpha}}^H$, and $\mathbf{F}_{\boldsymbol{\alpha},\boldsymbol{\omega}} = \mathbf{F}_{\boldsymbol{\omega},\boldsymbol{\alpha}}^H$.

Appendix C
Proof of Proposition 1

Since the FT bin does not influence the AoAs explicitly, we can let $N = 1$. Referring to Appendix A, the four submatrices in $\mathbf{F}_{\psi}$ are rewritten as

$$\mathbf{F}_{\boldsymbol{\nu},\boldsymbol{\nu}} = 2\sigma^{-2}\boldsymbol{\Lambda}^H\mathrm{Re}\{\boldsymbol{\Psi}'^H\mathbf{X}\boldsymbol{\Psi}'\}\boldsymbol{\Lambda}, \tag{52}$$

$$\mathbf{F}_{\boldsymbol{\nu},\boldsymbol{\tau}} = 2\sigma^{-2}\boldsymbol{\Lambda}^H\mathrm{Re}\{\boldsymbol{\Psi}'^H\mathbf{X}\boldsymbol{\Psi}''\}\boldsymbol{\Lambda}, \tag{53}$$

$$\mathbf{F}_{\boldsymbol{\tau},\boldsymbol{\tau}} = 2\sigma^{-2}\boldsymbol{\Lambda}^H\mathrm{Re}\{\boldsymbol{\Psi}''^H\mathbf{X}\boldsymbol{\Psi}''\}\boldsymbol{\Lambda}, \tag{54}$$

and $\mathbf{F}_{\boldsymbol{\tau},\boldsymbol{\nu}} = \mathbf{F}_{\boldsymbol{\nu},\boldsymbol{\tau}}^H$.

$$\mathbf{U}_{\rm nd} = \begin{bmatrix} u_1(2,1)^H(u_1(3,1)+u_1(1,1)) & \cdots & u_1(MG-1,1)^H(u_1(MG,1)+u_1(MG-2,1)) \\ u_1(2,1)^H(u_1(3,2)+u_1(1,2)) & \cdots & u_1(MG-1,1)^H(u_1(MG,2)+u_1(MG-1,2)) \\ \vdots & \vdots & \vdots \\ u_1(2,Q)^H(u_1(3,Q)+u_1(1,Q)) & \cdots & u_1(MG-1,Q)^H(u_1(MG,Q)+u_1(MG-2,Q)) \end{bmatrix}, \tag{57}$$

Supposed that $\mathbf{X}$ is a three-layer diagonal matrix, there are MG diagonal entries and $2(MG-1)$ non-diagonal entries. The dth diagonal entry is $x_d, d \in \{1, \cdots, MG\}$. The dth non-diagonal entry is $y_d, d \in \{1, \cdots, MG-1\}$.

Then, we can obtain the (q_1, q_2)th entry of $\mathbf{F}_{\boldsymbol{\nu},\boldsymbol{\nu}}$, $q_1, q_2 \in \{1, \cdots, Q\}$, as given by

$$\begin{aligned} \mathbf{F}_{\boldsymbol{\nu},\boldsymbol{\nu}}(q_1,q_2) =& 2\sigma^{-2}\mathrm{Re}\{\alpha_{q_1}^H \alpha_{q_2}\} \times \\ & \mathrm{Re}\left\{ \sum_{d=1}^{MG} x_d \boldsymbol{\Psi}'(d,q_1)^H \boldsymbol{\Psi}'(d,q_2) \right. \\ & + \sum_{d=1}^{MG-1} y_d \boldsymbol{\Psi}'(d,q_1)^H \boldsymbol{\Psi}'(d+1,q_2) \\ & \left. + \sum_{d=2}^{MG} y_d \boldsymbol{\Psi}'(d,q_1)^H \boldsymbol{\Psi}'(d-1,q_2) \right\}. \end{aligned} \tag{55}$$

Note that $\boldsymbol{\Psi}'$ has a dimension of $(MG) \times Q$. We denote $\boldsymbol{\Psi}'(d,q)$ as $u_1(d,q)$ and formulate two $Q^2 \times (MG-2)$ matrices, i.e.,

$$\mathbf{U}_{\rm d} = \begin{bmatrix} u_1^H(2,1)u_1(2,1) & \cdots & u_1^H(MG-1,1)u_1(MG-1,1) \\ \vdots & \vdots & \vdots \\ u_1^H(2,q')u_1(2,q) & \cdots & u_1^H(MG-1,q')u_1(MG-1,q) \\ \vdots & \vdots & \vdots \\ u_1^H(2,Q)u_1(2,Q) & \cdots & u_1^H(MG-1,Q)u_1(MG-1,Q) \end{bmatrix} \tag{56}$$

and $\mathbf{U}_{\rm nd}$ that is given by (57).

It is noted that $u_1(d,q)^H u_1(d,q)$ is not related to q, which means that there are Q rows in $\mathbf{U}_{\rm d}$ that are exactly the same. Additionally, $u_1(d,q_1)^H u_1(d,q_2)$ is the conjugate of $u_1(d,q_2)^H u_1(d,q_1)$. Hence, the number of independent rows of $\mathbf{U}_{\rm d}$ is at most $(Q^2-Q)/2+1$. For an arbitrary complex symmetric $\mathbf{F}_{\boldsymbol{v},\boldsymbol{v}}$ of dimension $Q \times Q$, the number of independent entries is $(Q^2-Q)/2+Q$, which is larger than $(Q^2-Q)/2+1$. This will cause that x_d can have no solution. The rank of $\mathbf{U}_{\rm nd}$ is Q^2 almost for sure. Hence, for an arbitrary $Q \times Q$ matrix $\mathbf{F}_{\boldsymbol{v},\boldsymbol{v}}$, both x_d and y_d are needed to guarantee the solution of the FT bin exists.

Note that we only use $\mathbf{F}_{\boldsymbol{v},\boldsymbol{v}}$ as an example. For a larger dimension FIM matrix, e.g., a $2Q \times 2Q$ matrix, we can formulate two matrices of dimension $4Q^2 \times (MG-2)$ with full rank and obtain the entries x_d and y_d accordingly, as long as MG is sufficiently larger than the Q^2. Therefore, the optimal non-limited FT bin matrix, $\mathbf{X}$, has three-layer non-zero diagonal entries.

REFERENCES

[1] A. R. Chiriyath, B. Paul, and D. W. Bliss, "Radar-communications convergence: Coexistence, cooperation, and co-design," *IEEE Trans. on Cogn. Commun. Netw.*, vol. 3, no. 1, pp. 1–12, Mar. 2017.

[2] F. Liu, C. Masouros, A. P. Petropulu, H. Griffiths, and L. Hanzo, "Joint radar and communication design: Applications, state-of-the-art, and the road ahead," *IEEE Trans. Commun.*, vol. 68, no. 6, pp. 3834–3862, Jun. 2020.

[3] P. Kumari, J. Choi, N. González-Prelcic, and R. W. Heath, "IEEE 802.11ad-based radar: An approach to joint vehicular communication-radar system," *IEEE Trans. Veh. Technol.*, vol. 67, no. 4, pp. 3012–3027, Apr. 2018.

[4] C. Sturm, Y. L. Sit, M. Braun, and T. Zwick, "Spectrally interleaved multi-carrier signals for radar network applications and multi-input multi-output radar," *IET Radar, Sonar Navigation*, vol. 7, no. 3, pp. 261–269, Mar. 2013.

[5] M. L. Rahman, P. Cui, J. A. Zhang, X. Huang, Y. J. Guo, and Z. Lu, "Joint communication and radar sensing in 5G mobile network by compressive sensing," in *2019 19th International Symposium on Communications and Information Technologies (ISCIT)*, Sep. 2019, pp. 599–604.

[6] M. L. Rahman, J. A. Zhang, X. Huang, Y. J. Guo, and R. W. Heath, "Framework for a perceptive mobile network using joint communication and radar sensing," *IEEE Trans. Aerosp. Electron. Syst.*, vol. 56, no. 3, pp. 1926–1941, Jun. 2020.

[7] J. A. Zhang, M. L. Rahman, K. Wu, X. Huang, Y. J. Guo, S. Chen, and J. Yuan, "Enabling joint communication and radar sensing in mobile networks—a survey," *IEEE Communications Surveys & Tutorials*, vol. 24, no. 1, pp. 306–345, 2022.

[8] Z. Ni, J. A. Zhang, X. Huang, K. Yang, and J. Yuan, "Uplink sensing in perceptive mobile networks with asynchronous transceivers," *IEEE Trans. Signal Process.*, vol. 69, pp. 1287–1300, 2021.

[9] J. A. Zhang, A. Cantoni, X. Huang, Y. J. Guo, and R. W. Heath, "Framework for an innovative perceptive mobile network using joint communication and sensing," in *2017 IEEE 85th Vehicular Technology Conference (VTC Spring)*, Jun. 2017, pp. 1–5.

[10] S. Huang, M. Zhang, Y. Gao, and Z. Feng, "Mimo radar aided mmwave time-varying channel estimation in MU-MIMO V2X communications," *IEEE Trans. Wireless Commun.*, vol. 20, no. 11, pp. 7581–7594, 2021.

[11] C. Li, N. Raymondi, B. Xia, and A. Sabharwal, "Outer bounds for a joint communicating radar (comm-radar): The uplink case," *IEEE Trans. Commun.*, vol. 70, no. 2, pp. 1197–1213, 2021.

[12] X. Zhang, L. Xu, L. Xu, and D. Xu, "Direction of departure (DOD) and direction of arrival (DOA) estimation in MIMO radar with reduced-dimension MUSIC," *IEEE Commun. Lett.*, vol. 14, no. 12, pp. 1161–1163, 2010.

[13] J. Gu, J. Moghaddasi, and K. Wu, "Delay and Doppler shift estimation for OFDM-based radar-radio (RadCom) system," in *2015 IEEE International Wireless Symposium (IWS 2015)*, Mar. 2015, pp. 1–4.

[14] O. Mehanna and N. D. Sidiropoulos, "Maximum likelihood passive and active sensing of wideband power spectra from few bits," *IEEE Trans. Signal Process.*, vol. 63, no. 6, pp. 1391–1403, 2015.

[15] Y. Liu, G. Liao, J. Xu, Z. Yang, and Y. Zhang, "Adaptive OFDM integrated radar and communications waveform design based on information theory," *IEEE Commun. Lett.*, vol. 21, no. 10, pp. 2174–2177, Oct. 2017.

[16] A. Turlapaty and Y. Jin, "A joint design of transmit waveforms for radar and communications systems in coexistence," in *2014 IEEE Radar Conference*, 2014, pp. 0315–0319.

[17] Y. L. Sit, B. Nuss, and T. Zwick, "On mutual interference cancellation in a MIMO OFDM multiuser radar-communication network," *IEEE Trans. Veh. Technol.*, vol. 67, no. 4, pp. 3339–3348, Apr. 2018.

[18] F. Liu, C. Masouros, A. Li, H. Sun, and L. Hanzo, "MU-MIMO communications with MIMO radar: From co-existence to joint transmission,"

IEEE Trans. Wireless Commun., vol. 17, no. 4, pp. 2755–2770, Apr. 2018.
[19] B. Li and A. Petropulu, "MIMO radar and communication spectrum sharing with clutter mitigation," in *2016 IEEE Radar Conference (RadarConf)*, May 2016, pp. 1–6.
[20] B. Li, A. P. Petropulu, and W. Trappe, "Optimum co-design for spectrum sharing between matrix completion based MIMO radars and a MIMO communication system," *IEEE Trans. Signal Process.*, vol. 64, no. 17, pp. 4562–4575, Sep. 2016.
[21] D. Tagliaferri, M. Mizmizi, S. Mura, F. Linsalata, D. Scazzoli, D. Badini, M. Magarini, and U. Spagnolini, "Integrated sensing and communication system via dual-domain waveform superposition," *arXiv preprint arXiv:2212.07950*, 2022.
[22] Z. Huang, A. Liu, R. Du, and T. X. Han, "Capacity-CRB tradeoff in OFDM integrated sensing and communication systems," in *ICC 2023-IEEE International Conference on Communications*. IEEE, 2023, pp. 2437–2442.
[23] M. D. Larsen, A. L. Swindlehurst, and T. Svantesson, "Performance bounds for MIMO-OFDM channel estimation," *IEEE Trans. Signal Process.*, vol. 57, no. 5, pp. 1901–1916, May 2009.
[24] B. Tang, J. Tang, and Y. Peng, "Waveform optimization for MIMO radar in colored noise: Further results for estimation-oriented criteria," *IEEE Trans. Signal Process.*, vol. 60, no. 3, pp. 1517–1522, 2012.
[25] S. Sodagari, A. Khawar, T. C. Clancy, and R. McGwier, "A projection based approach for radar and telecommunication systems coexistence," in *2012 IEEE Global Communications Conference (GLOBECOM)*, Dec. 2012, pp. 5010–5014.
[26] X. Wang, Z. Fei, J. A. Zhang, and J. Xu, "Partially-connected hybrid beamforming design for integrated sensing and communication systems," *IEEE Trans. Commun.*, vol. 70, no. 10, pp. 6648–6660, 2022.
[27] L. Xu, J. Li, P. Stoica, K. W. Forsythe, and D. W. Bliss, "Waveform optimization for MIMO radar: A Cramér-Rao bound based study," in *2007 IEEE International Conference on Acoustics, Speech and Signal Processing - ICASSP '07*, vol. 2, 2007, pp. II–917–II–920.
[28] K. Qian, C. Wu, Y. Zhang, G. Zhang, Z. Yang, and Y. Liu, "Widar2.0: Passive human tracking with a single Wi-Fi link," in *Proceedings of the 16th Annual International Conference on Mobile Systems, Applications, and Services*. New York, NY, USA: Association for Computing Machinery, 2018, pp. 350–361. [Online]. Available: https://doi.org/10.1145/3210240.3210314.
[29] A. Kumar, D. Singh, H. D. Joshi, A. K. Singh, W. Anwar, T. Myllyla, and M. Magarini, "Generalized adaptive spreading modulation: A novel waveform for integrated sensing and communication oriented vehicular applications," *Authorea Preprints*, 2023.

Zhitong Ni (Member, IEEE) received the B.E. degree in information engineering from Beijing Institute of Technology (BIT), Beijing, China, in 2017, and received the dual Ph.D. degree from University of Technology Sydney (UTS), Sydney, Australia, and BIT, Beijing, China in 2022 and 2023, respectively. He is currently working as a Research Associate with the Global Big Data Technologies Centre, UTS. His research interests include array signal processing, channel parameter estimations, as well as precoding techniques in various applications including the sixth-generation cellular systems and integrated radio sensing and communication (ISAC) systems.

J. Andrew Zhang (M'04-SM'11) received the B.Sc. degree from Xi'an JiaoTong University, China, in 1996, the M.Sc. degree from Nanjing University of Posts and Telecommunications, China, in 1999, and the Ph.D. degree from the Australian National University, Australia, in 2004.

Currently, Dr. Zhang is a Professor in the School of Electrical and Data Engineering, University of Technology Sydney, Australia. He was a researcher with Data61, CSIRO, Australia from 2010 to 2016, the Networked Systems, NICTA, Australia from 2004 to 2010, and ZTE Corp., Nanjing, China from 1999 to 2001. Dr. Zhang's research interests are in the area of signal processing for wireless communications and sensing, with a focus on integrated sensing and communications. He has published more than 300 papers in leading Journals and conference proceedings, and has won 5 best paper awards for his work including in IEEE ICC2013. He is a recipient of CSIRO Chair's Medal and the Australian Engineering Innovation Award in 2012 for exceptional research achievements in multi-gigabit wireless communications.

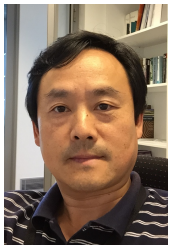

Xiaojing Huang (M'99-SM'11) received the B.Eng., M.Eng., and Ph.D. degrees in electronic engineering from Shanghai Jiao Tong University, Shanghai, China, in 1983, 1986, and 1989, respectively. He was a Principal Research Engineer with the Motorola Australian Research Center, Botany, NSW, Australia, from 1998 to 2003, and an Associate Professor with the University of Wollongong, Wollongong, NSW, Australia, from 2004 to 2008. He had been a Principal Research Scientist with the Commonwealth Scientific and Industrial Research Organisation (CSIRO), Sydney, NSW, Australia, and the Project Leader of the CSIRO Microwave and mm-Wave Backhaul projects since 2009. He is currently a Professor of Information and Communications Technology with the School of Electrical and Data Engineering and the Program Leader for Mobile Sensing and Communications with the Global Big Data Technologies Center, University of Technology Sydney (UTS), Sydney, NSW, Australia. His research interests include high-speed wireless communications, digital and analog signal processing, and synthetic aperture radar imaging. With over 32 years of combined industrial, academic, and scientific research experience, he has authored over 330 book chapters, refereed journal and conference papers, major commercial research reports, and filed 31 patents. Prof. Huang was a recipient of the CSIRO Chairman's Medal and the Australian Engineering Innovation Award in 2012 for exceptional research achievements in multigigabit wireless communications.

Ren Ping Liu (Senior Member, IEEE) received the B.E. and M.E. degrees from the Beijing University of Posts and Telecommunications, China, and the Ph.D. degree from The University of Newcastle, Australia. He is currently a Professor and the Head of Discipline of Network and Cybersecurity at the University of Technology Sydney (UTS). Since joining UTS in 2016, he has received 18 research grants (led 12) totaling over 5 million dollars. As a Research Leader, a Certified Network Professional, and a Full Stack Web Developer, he has delivered networking and cybersecurity solutions to a number of government agencies and industry customers. He has supervised over 30 Ph.D. students and has over 200 research publications. His research interests include wireless networking, 5G, the IoT, vehicular networks, 6G, cybersecurity, and blockchain. Prof. Liu was the Winner of NSW iAwards 2020 for leading the Blockchain enabled Fish provenance And Quality Tracking (BeFAQT) Project. He was awarded the Australian Engineering Innovation Award in 2012 and CSIRO Chairman's Medal for his contribution in the Wireless Backhaul Project. He was the Founding Chair of IEEE NSW VTS Chapter. He served as the technical program committee chairs and organizing committee chairs in a number of IEEE conferences.